Chemical evolution of primary and secondary biomass burning aerosols during daytime and nighttime

Amir Yazdani[1], Satoshi Takahama[1], John K. Kodros[2], Marco Paglione[2,3], Mauro Masiol[2], Stefania Squizzato[2], Kalliopi Florou[2], Christos Kaltsonoudis[2], Spiro D. Jorga[2], Spyros N. Pandis[2,4], and Athanasios Nenes[1,2]

[1]Laboratory of atmospheric processes and their impacts (LAPI), ENAC/IIE, Ecole polytechnique fédérale de Lausanne (EPFL), Lausanne, Switzerland
[2]Institute for Chemical Engineering Sciences, Foundation for Research and Technology Hellas (ICE-HT/FORTH), Patra, Greece
[3]Italian National Research Council - Institute of Atmospheric Sciences and Climate (CNR-ISAC), Bologna, Italy
[4]Department of Chemical Engineering, University of Patras, Patra, Greece

Correspondence: Satoshi Takahama (satoshi.takahama@epfl.ch), Athanasios Nenes (athanasios.nenes@epfl.ch)

Abstract.

Primary emissions from wood and pellet stoves were aged in an atmospheric simulation chamber under daytime and nighttime conditions. The aerosol was analyzed with the online Aerosol Mass Spectrometer (AMS) and offline Fourier transform infrared spectroscopy (FTIR). Measurements using the two techniques agreed reasonably well in terms of the organic aerosol (OA) mass concentration, OA:OC trends, and concentrations of biomass burning markers – lignin-like compounds and anhydrosugars. Based on the AMS, around 15 % of the primary organic aerosol (POA) mass underwent some form of transformation during daytime oxidation conditions after 6–10 hours of atmospheric exposure. A lesser extent of transformation was observed during the nighttime oxidation. The decay of certain semi-volatile (e.g., levoglucosan) and less volatile (e.g., lignin-like) POA components was substantial during aging, highlighting the role of heterogeneous reactions and gas-particle partitioning. Lignin-like compounds were observed to degrade under both daytime and nighttime conditions, whereas anhydrosugars degraded only under daytime conditions. Among the marker mass fragments of primary biomass burning OA (bbPOA), heavy ones (higher m/z) were relatively more stable during aging. The biomass burning secondary OA (bbSOA) became more oxidized with continued aging and resembled those of aged atmospheric organic aerosols. The bbSOA formed during daytime oxidation was dominated by acids. Organonitrates were an important product of nighttime reactions in both humid and dry conditions. Our results underline the importance of changes to both the primary and secondary biomass burning aerosols during their atmospheric aging. Heavier AMS fragments seldomly used in atmospheric chemistry can be used as more stable tracers of bbPOA and in combination with the established levoglucosan marker, can provide an indication of the extent of bbPOA aging.

1 Introduction

Fine particulate matter (PM) in the atmosphere impacts climate and visibility (McFiggans et al., 2004; Hallquist et al., 2009) and is known to cause respiratory and cardiovascular diseases, leading to premature mortality (Pope et al., 2009; Shiraiwa et al.,

2017; Burnett et al., 2018). A major fraction (up to 90 %) of fine PM is organic. Organic aerosol (OA) has various sources and formation mechanisms in the atmosphere, resulting in its complex chemical composition (Russell, 2003; Kanakidou et al., 2005; Hallquist et al., 2009). Primary organic aerosols (POA) are emitted directly from their sources, whereas secondary organic aerosols (SOA) are formed through chemical reactions of organic vapors that produce lower-volatility compounds

25 (Seinfeld and Pandis, 2016). Oxygenated OA often dominates atmospheric OA, highlighting the importance of atmospheric chemistry and aging for OA (Zhang et al., 2007) as particles and gases are exposed to oxidants for days in the atmosphere (Wang et al., 2018). The major types of aging include: homogeneous gas-phase oxidation and condensation (Donahue et al., 2012), oligomerization (Kalberer et al., 2006), heterogeneous reactions with oxidants (Robinson et al., 2006; George et al., 2008), and photolysis (Bateman et al., 2011; Henry and Donahue, 2012). Oxidation reactions by excited state photosensitizers can

30 also lead to SOA formation and composition changes in OA (Tsui and McNeill, 2018; Mabato et al., 2022; Zhang et al., 2022). Homogeneous gas-phase reactions are generally believed to dominate (Henry and Donahue, 2012), while other mechanisms may be important under different conditions (e.g., Hearn et al., 2005; Hung et al., 2005; Nah et al., 2014).

Biomass burning (BB) contributes significantly to atmospheric primary and secondary OA (POA and SOA) (Puxbaum et al., 2007; Qi et al., 2019; Lanz et al., 2010), brown and black carbon (BrC and BC, respectively) (Bond et al., 2013).

35 BB is expected to have an increasing contribution to $PM_{2.5}$ in the foreseeable future (Ford et al., 2018). Primary (bbPOA) and secondary bbOA (bbSOA) formed during reactions with hydroxyl and nitrate radicals have been investigated in several environmental chamber and field studies (Johansson et al., 2004; Bäfver et al., 2011; Alves et al., 2011; Hennigan et al., 2011; Bruns et al., 2015; Tiitta et al., 2016; Bertrand et al., 2017, 2018a; Kodros et al., 2020; Jorga et al., 2021; Yazdani et al., 2021a). These studies have suggested a net enhancement in the OA concentration with aging due to bbSOA formation. To estimate

40 the contributions of bbPOA and bbSOA after aging in chamber or in field measurements, bbPOA implicitly (e.g., when using positive matrix factorization) or explicitly is assumed to be stable during the aging (Robinson et al., 2007; Grieshop et al., 2009; Tiitta et al., 2016; Kodros et al., 2020), neglecting the effects of heterogeneous reactions, photolysis, and the changing gas-particle partitioning of its components. This is an approximation, given that several studies report significant degradation of bbPOA markers like anhydrosugars and methoxyphenols during aging (Hennigan et al., 2010, 2011; Slade and Knopf, 2013;

45 Bertrand et al., 2018a; Yazdani et al., 2021c). These compounds constitute a significant fraction (up to 50 %) of the bbPOA mass (Fine et al., 2002; Bertrand et al., 2018a; Yazdani et al., 2021c). This chemical processing can impact the bbPOA mass and composition significantly, but has not been well-characterized to date.

Recent efforts using the volatility basis set (VBS; Donahue et al., 2006) address the volatility and gas-particle partitioning of POA including primary bbOA in simulations (Robinson et al., 2007; Theodoritsi et al., 2020). However, the chemical

50 processing of bbPOA remains uncertain and heterogeneous reactions of bbOA compounds are not included in most models.

Aerosol mass spectrometry (AMS) and Fourier transform infrared spectroscopy (FTIR) are two methods used in this work to study the bbOA composition and its evolution with aging. AMS, while being capable of analyzing most of the OA mass (Hallquist et al., 2009), is limited by the extensive molecule fragmentation and the variability of particle collection efficiency (CE)(Canagaratna et al., 2007; Faber et al., 2017; Kumar et al., 2018). FTIR is a non-destructive method that measures the

55 abundance of certain functional groups but with a limited temporal resolution. Functional group abundances are then used to

estimate the OA mass concentration and elemental ratios (Coury and Dillner, 2008; Ruthenburg et al., 2014; Reggente et al., 2016; Boris et al., 2019). A recent study also shows the ability of FTIR to quantify bbOA marker molecules (Yazdani et al., 2021c).

In this work, primary biomass burning emissions generated from pellet and wood stoves are injected into an environmental simulation chamber and aged with hydroxyl and nitrate radicals. AMS and FTIR are used in tandem to better understand and quantify the evolution of primary and the formation of secondary bbOA with aging. We adopt a particle wall loss correction method based on AMS organic measurements and develop a procedure to quantify the overall changes in the composition of bbPOA during the coarse of aging with AMS and FTIR. The results of this study allow us to evaluate the stability of bbPOA under different conditions, the usefulness of different markers to identify aged atmospheric bbOA, and the importance of aging mechanisms other than the homogeneous gas-phase oxidation under atmospherically relevant conditions.

2 Methods

2.1 Experimental set-up and procedure

Primary emissions from common wood and pellet stoves were diluted and injected for 30–40 min into a 10 m^3 Teflon atmospheric simulation chamber located at the Foundation for Research and Technology-Hellas (FORTH), Greece. Olive wood logs with bark and EN*plus*® A1 pellets were used as fuel. Details of the chamber and combustion facilities have been discussed elsewhere (Kaltsonoudis et al., 2017; Kodros et al., 2020). The fuels and stoves used in this work are commonly used in the region. Primary emissions were left in the chamber after the injection for around two hours to ensure proper mixing and to characterize chamber wall losses.

Nine experiments were conducted in this work. For the three reference experiments (Table 1), emissions were left in the dark chamber without addition of any oxidants. For the two experiments simulating daytime aging, reactions were initiated by turning on UV ~~lights~~ fluorescent lamps (Osram, L 36W/73) ($J_{NO_2} = 0.59$ min^{-1}) and the subsequent generation of the hydroxyl radical via ozone photolysis in the presence of water vapor for around 2 h. For these experiments the average RH was roughly 50 % and the average OH concentration was $(3–5)\times10^6$ molecule cm^{-3}. This corresponds to 6–10 h of aging in the atmosphere assuming an average OH concentration of 10^6 molecule cm^{-3} (Seinfeld and Pandis, 2016). The OH concentration was estimated using a proton-transfer-reaction mass spectrometer (PTRMS, Ionicon Analytik) monitoring the concentration of 1-butanol-d9 injected initially into the chamber (Barmet et al., 2012). The four nocturnal aging experiments were conducted under two different RH regimes: dry (10 %) and humid (60–80 %). For these experiments, roughly 100 ppb of NO_2 was injected into the chamber before the primary biomass burning emissions. Around two hours after the injection of primary emissions, aging was initiated by injection of O_3 (roughly 100 ppb) and production of the NO_3 radical via the reaction of O_3 with NO_2. Both NO_2 and O_3 concentrations were measured by Teledyne gas monitors.

2.2 On- and off-line PM measurements

The composition of non-refractory aerosols in the chamber was measured by a HR-ToF AMS (Aerodyne Research Inc.) operating in V mode. For certain experiments, the AMS also measured the composition of chamber aerosols after being passed through a thermodenuder to study their volatility. A scanning mobility particle sizer (classifier model 3080, DMA model 3081, CPC model 3787, TSI) was used to measure the particle number size distribution in the 15–700 nm range. Primary and aged PM_1 were collected on 47 mm PTFE filters (Pall corporation, 1 cm diameter of the collection surface). Sampling on PTFE filters was performed at a flow rate of $8 \, L \, min^{-1}$ for 20 min using a flow system composed of a silica gel denuder to minimize aerosol water and a sharp-cut-off cyclone. Filters were immediately stored in petri dishes at 253 K to minimize volatilization of aerosols and chemical reactions. Filter samples were analyzed using a Bruker Vertex 80 FTIR instrument equipped with a α deuterated lanthanum alanine doped triglycine sulfate (DLaTGS) detector and a custom-made filter mini-chamber to minimize water vapor and CO_2 interferences. The spectra were obtained at a resolution of $4 \, cm^{-1}$ and were averaged over 128 scans.

2.3 Data analysis

2.3.1 Initial spectral post-processing

The AMS raw signal was post-processed using the AMS software toolkits SeQUential Igor data RetRiEvaL (SQUIRREL) v1.57 and the Peak Integration by Key Analysis (PIKA) v1.16. The elemental and OA:OC ratios were calculated using the approach of Canagaratna et al. (2015). The organic nitrate concentration was calculated based on NO^+ and NO_2^+ peak ratios in the AMS mass spectra following the approach of Farmer et al. (2010).

Baseline correction was performed on the FTIR spectra to eliminate the contribution of light scattering from the spectra (Russo et al., 2014; Parks et al., 2019) using smoothing splines. After baseline correction, blank subtraction was performed to recover some of the overlapping features with PTFE peaks (e.g., levoglucosan fingerprint bands 860–1050 cm^{-1}). A multiple peak-fitting algorithm was applied on the FTIR spectra to estimate ~~abundances of~~ the contribution of absorption related to alcohol (referred to as aCOH), carboxylic acid (COOH), alkane (aCH), and non-acid carbonyl (naCO) groups (Takahama et al., 2013). The area under each peak was related to the abundance of the corresponding functional group using the measured absorption coefficient by Reggente et al. (2019).

The ratio of fingerprint absorbances related to levoglucosan (multiple peaks in the 860–1050 cm^{-1} range; Yazdani et al., 2021c) ~~and lignin-like compounds (single sharp peak at 1515)~~ in the FTIR spectra were compared between primary and aged aerosols to estimate the change of ~~these two biomass burning markers~~ this biomass burning marker with aging. Absolute levoglucosan concentrations were estimated ~~using the mentioned fingerprint absorbances, with~~ by averaging the heights of each of the three peaks in the fingerprint region and applying absorption coefficient estimated from measurements of ~~Ruthenburg et al. (2014).~~ Ruthenburg et al. (2014). The peak heights were defined relative to a local baseline defined by a linear interpolation among peak valleys (Yazdani, 2022).

The single sharp peak at 1515 cm^{-1} related to lignin-like compounds was used to estimate and compare the concentration of this group of compounds in primary and aged aerosols. Due to the lack absorption coefficient for the 1515 cm^{-1} peak, the

following approach was taken to estimate the concentration of lignin-like compounds: Fine et al. (2002) found syringaldehyde
to be one of the most abundant lignin-like compounds in bbPOA. The total concentration of lignin-like compounds was esti-
mated using the absorption coefficient of the 1515 cm^{-1} peak for syringaldehyde. As this coefficient was not ~~measured~~availble
in the literature, it was calculated by scaling the measured coefficient of carbonyl ~~Reggente et al. (2019)~~ (Reggente et al., 2019)
by the ratio of absorbances at 1515 and 1680 cm^{-1} from a spectrum of the compound prepared in potassium bromide wafer
taken from a reference database ~~2022~~(SpectraBase, John Wiley & Sons, Inc., 2022).

2.3.2 Quantifying the bbPOA transformation

Particle wall loss correction for AMS and FTIR measurements was carried out assuming a first-order, time independent wall
loss rate constant for the OA mass concentration (Pathak et al., 2007):

$$\ln\left[C_{\mathrm{OA}}(t)\right] = -k_{\mathrm{OA}}\,t + \ln\left[C_{\mathrm{OA}}(0)\right], \tag{1}$$

where k_{OA} is the wall loss rate constant and C_{OA} is the AMS OA mass concentration. The rate constant for each experiment
was calculated using OA concentrations from 0.5–1 h after the injection of primary emissions into the chamber (to ensure
proper mixing) up to the start of chemical aging or until the end for reference experiments. Wall-loss-corrected concentrations
of individual AMS fragments were calculated by:

$$C_i^{\mathrm{cor}}(t) = C_i^{\mathrm{obs}}(t) + k_{\mathrm{OA}} \int_0^t C_i^{\mathrm{obs}}(t)\,dt, \tag{2}$$

where $C_i^{\mathrm{obs}}(t)$ is the measured concentration of fragment i at time t, and $C_i^{\mathrm{cor}}(t)$ is its wall-loss-corrected concentration at
time t. In this process, it is assumed that particles are internally mixed and there is a minor size dependence for the chemical
composition of bbOA. These assumptions are supported by the measurements of Grieshop et al. (2009). The difference between
the wall-loss corrected and initial concentrations of diminishing fragments (those with $C_i^{\mathrm{cor}}(t) - C_i^{\mathrm{cor}}(0) < 0$) was used to
quantify the extent of bbPOA transformation at each time after the start of aging with AMS.

2.3.3 Residual spectra

The apparent contribution of the fresh bbPOA to aged bbOA spectra (FTIR or AMS) was calculated using Eq. (3) assuming no
evaporation, condensation, or heterogeneous reactions:

$$\boldsymbol{s}_{\mathrm{bbPOA}}(t) = \boldsymbol{s}_{\mathrm{bbPOA}}(0)\exp(-k_{\mathrm{OA}}t), \tag{3}$$

where $\boldsymbol{s}_{\mathrm{bbPOA}}(t)$ is the apparent bbPOA spectrum at time t, and $\boldsymbol{s}_{\mathrm{bbPOA}}(0)$ is the bbPOA spectrum at the start of aging. The
residual spectrum at time t, ~~$\boldsymbol{s}_{\mathrm{res}}(0)$~~$\boldsymbol{s}_{\mathrm{res}}(t)$, was defined as the result of subtraction of the apparent bbPOA spectrum at time t
from that of the aged bbOA:

$$\boldsymbol{s}_{\mathrm{res}}(t) = \boldsymbol{s}_{\mathrm{bbOA}}(t) - \boldsymbol{s}_{\mathrm{bbPOA}}(t). \tag{4}$$

The FTIR and AMS residual spectra are composed of positive and negative elements. The positive elements, which indicate the formation of bbSOA species or oxidation products of fresh bbPOA, were studied in both AMS and FTIR residual spectra. The negative elements, on the other hand, indicate the loss of fresh bbPOA species. The negative peaks in the FTIR residual spectra were used to obtain another estimate of bbPOA transformation with aging that does not suffer from the limitations of the AMS.

2.3.4 Dimension reduction of AMS spectra

We used principal component analysis (PCA; Hotelling, 1933) to simplify the high-dimensional, inter-correlated AMS spectra, while considering variations in the majority of mass fragments. This allows the better understanding of the evolution of bbOA during the course of aging in the chamber and to compare it to atmospheric aerosols. PCA calculations were performed on the normalized (by the total AMS OA concentration) and uncentered AMS spectra from the chamber experiments (1600 spectra with 800 fragments) using singular value decomposition (Abdi and Williams, 2010). Thereafter, positive matrix factorization (PMF) factors of atmospheric OA from previous studies (e.g., Aiken et al., 2009) were projected onto the PC space for comparison.

3 Results

The composition of bbPOA and extent of aging in these experiments is described in Sect. 3.1. We discuss the range of estimated wall loss correction factors and uncertainties in Sect. 3.2, and, taking them into consideration, describe the results of each type of experiment in Sects. 3.3–3.5.

3.1 General description of primary biomass burning organic aerosols and extent of aging

The FTIR spectral profiles of primary wood and pellet burning aerosols are generally similar (Fig. 1). However, the higher relative absorbances of levoglucosan and the alcohol group, and the lower absorbance of lignin-like compounds stand out for the pellet burning aerosols. Primary pellet burning aerosols also have similar FTIR spectra to that of wood (Pandey, 1999) but have higher relative concentrations of aCOH and levoglucosan compared to wood burning aerosols (Fig. 1) that can be attributed to different combustion conditions and OA concentrations between the two fuels. For wood and pellet fuels, different ratios of lignin-related fragments (e.g., $C_8H_9O_2^+$, $C_9H_{11}O_3^+$, $C_{10}H_{13}O_3^+$; Li et al., 2012; Tolbert and Ragauskas, 2017; Bertrand et al., 2017) are observed, reflecting different composition of the fuels and combustion conditions (e.g., combustion efficiency). We also observe that the relative abundance of lignin- and levoglucosan-related fragments and their corresponding FTIR absorbances vary among different experiments with the same fuel probably due to slightly different combustion conditions.

As stated in the previous Section, OA concentrations of AMS (without CE correction) and FTIR were correlated $R^2 = 0.75$, with . The OM:OC also showing estimated using these two also showed similar trends upon aging (Supplement S3). The spectral features and chemical composition of primary wood burning aerosols from FTIR — and mass fragment profiles from

AMS — in this work are consistent with that previously reported (e.g., Tiitta et al., 2016; Bertrand et al., 2017, 2018a; Yazdani et al., 2021c). The FTIR spectra of these primary aerosols largely resemble that of wood constituents such as lignin (Yazdani et al., 2021c). However, The aCH peaks are more prominent in the FTIR spectra of wood burning aerosols of this work compared to those of Yazdani et al. (2021c) likely due to the combustion of wood with bark.

Visualizing the evolution of f_{44}-f_{43} ($f_{CO_2^+}$-$f_{C_2H_3O^+}$) and the first three ~~principle~~ principal components compares the extent to which primary and residual bbOA in these chamber experiments are similar to the atmospheric bbOA and OOA factors, respectively. As can be seen from Fig. 2, the trajectory for the total bbOA spans a small range of the plot and is located in the lower section of the triangle (Ng et al., 2011). For the residual OA formed using UV lights, however, the trajectories start in the lower section of the triangle and continue upward until they end close to the upper vertex. The end points are also close to the location of the OOA factor for atmospheric aerosols collected in Finokalia, Greece (Florou, *manuscript in preparation*, ~~2022~~2023). The latter suggests that the extent of aging by UV in the chamber is comparable to that observed in the atmosphere.

The residual OA from wood and pellet burning emissions aged ~~with the nitrate radical in~~ in dark and dry conditions occupy the lower part of the triangle plot with a relatively less significant change in f_{44} and f_{43} with aging (Fig. 2)~~. In humid conditionswith the nitrate radical~~, implying only mild oxidation. Contrary to dark and dry conditions, in dark and humid conditions, the trajectories resemble more those of UV experiments~~except for the elevated~~. The f_{44} and f_{43} ~~(Fig. 2), suggesting the importance of aqueous nitrate radical reactions for oxidizing bbOA~~ increases more significantly, suggesting a stronger oxidation due to aqueous (nitrate radical) reactions. f_{43} is more elevated for aged bbOA in dark and humid conditions compared to those aged using UV (Fig. 2). The latter has also been observed by Kodros et al. (2020) and Kodros et al. (2022). Although the general oxidation trend is observed to be similar between PB and WB OA in dark conditions, the length of oxidation trajectories and their starting point appear to be somewhat different. These differences are believed to be related to different levels of aging in different experiments and slightly different composition of fresh PB and WB OA, respectively.

PCA extends the ~~AMS analysis to consider~~ analysis of AMS spectra to additional fragments besides CO_2^+ and $C_2H_3O^+$. ~~Principle~~ Principal components (PCs) were derived from chamber AMS spectra to highlight mass fragments describing most of variation in the chamber AMS spectra. Thereafter, the residual chamber spectra and atmospheric PMF factors from Mexico City 2009 and Finokalia (Florou, *manuscript in preparation*, ~~2022~~2023) were projected onto the PC space including the first three PCs (Fig. 3). ~~Closeness of points in the PC space implies their spectral similarity. The~~ Since the first three principal components (PCs) in Fig. 3, describe the majority (87%) of the total variance in AMS spectra, similar PC scores (closeness of points) implies their spectral similarity. These PCs have high loadings only for few fragments, making their interpretation straightforward (Supplement S4). PC1 mainly indicates the general direction of aging, PC2 indicates the abundance of the CHO$^+$ fragment (usually considered as a surrogate for alcohols), and PC3 captures the degradation of biomass burning markers (e.g., levoglucosan) with aging (~~Section S4~~Supplement S4). As can be seen in Fig. 3, the atmospheric bbOA factor from Aiken et al. (2009) is located close to the primary wood burning aerosols in ~~the PC space~~both plots, suggesting their similar composition. The residual OA formed ~~by the nitrate radical in dry conditions is~~ in dark and dry conditions appears to be the least aged among all (~~e.g.,~~ residual spectra with higher PC1 loading~~)~~, and is located closer to aged chamber OA. The residual OA aged ~~with the nitrate radical in~~ in dark and humid conditions is, however, ~~more aged~~ to be more oxidized than that in dry

conditions, and it is located closer to the atmospheric semi-volatile OA factor (OOA-2). The residual OA in the UV experiment has the most aged spectrum and is located the closest to the atmospheric low-volatility oxygenated OA (OOA-1) in the PC1-

215 PC2 and PC1-PC3 biplots (Fig. 3). The results of the PCA analysis support those of the f_{44}-f_{43} plot in terms of similarity of aged chamber aerosols to field measurements, while considering a wider range of mass fragments. Additionally, the PCA analysis ~~indicates~~ characterizes the functional group content of aerosols discussed in this and following sections using fewer variables. For example, as can be seen in Fig. 3, pellet burning aerosols have higher PC2 scores compared to wood burning, consistent with the higher alcohol content observed in their FTIR spectra (Fig. 1).

220 ## 3.2 Wall loss corrections

The procedure for obtaining wall loss coefficients for correction of mass fragment profiles and residual spectra of AMS and FTIR is illustrated here for a UV experiment (experiment 5). First, a first-order loss is fitted to the AMS OA concentration before the start of aging (in the -1.5–0 h range). The first order model explains the OA trend in this experiment with $R^2 = 0.95$. The fitted curve is shown by a dashed curve in Fig. 4.

225 The estimated wall loss correction coefficients range from 0.06–0.11 with an estimated uncertainty of 5–12% (Table 2). The first-order wall loss model is able to explain well ($R^2 > 0.8$) the overall variations in the AMS OA concentration for the reference experiments and the period prior to initiation of aging for other experiments (Section S1). In addition, the decrease in the OA concentration estimated with FTIR for the reference experiments closely matches (less than 5% difference) that with AMS (bbPOA ratios shown in Table 2). The latter supports the wall loss rate constants derived from AMS OA. Systematic

230 differences up to 15% are observed between the diminution of different fragments in reference experiments (Fig. 5a), which are investigated further in Sect. 3.3. These differences are relatively small compared to those in experiments with oxidants (Sects. 3.4–3.5).

3.3 Reference experiment

Interpretation of experiments in this and remaining sections are primarily made on wall-loss-corrected AMS fragments normal-

235 ized by their concentrations at the start of aging. The trends were observed to be similar within each aging scenario regardless of the fuel burned, so an experiment representing each category is shown in Fig. 5. The increase in the normalized concentration of fragments (usually oxygenated fragments) indicates the appearance of new species, for example, through SOA condensation. A decrease in the normalized concentrations suggests that certain species diminish with aging either due to heterogeneous reactions or evaporation. Residual AMS and FTIR spectra for each category (Figs. 6 and 7) provides further support of conclusions

240 drawn from the wall-loss-corrected time series profiles of AMS fragments.

As can be seen from Fig. 5a, in the reference experiment 1, wall-loss corrected fragments follow the general temporal trend of the total OA, with deviations within 10%. Mass fragment concentrations in the residual AMS and absorbances in the residual FTIR spectra are noisy and close-to-zero (Figs. 6a and 7a), implying negligible emergence of new species. The loss of levoglucosan in experiment 2 with RH around 50%, however, results in high uncertainty for its corresponding fragment,

245 $C_2H_4O_2^+$, in Fig. 6a. This observation suggests that the composition of OA does not change noticeably in the absence of

oxidants; less than 2 % of bbPOA mass is transformed after leaving the emissions in the chamber for around 4 h. This value can be considered as a baseline for other aging scenarios.

Some species-specific changes can be detected in these experiments. For instance, the systematic negative trend in the fragment attributed to levoglucosan (and anhydrosugars) $C_2H_4O_2^+$ and positive trend in a fragment related to lignin-like com-
250 pounds $C_9H_{11}O_3^+$ that can be viewed in Figure 5a indicates that their rate of loss in the chamber is greater than and less than total OA, respectively, since the wall-loss correction is based on the OA. $C_2H_4O_2^+$ and small $C_xH_y^+$ fragments (e.g., CH_2^+, $C_2H_2^+$, $C_4H_6^+$) appear to have a higher-than-average loss rates, while the fragments attributed to lignin-related compounds appear to diminish less. Similar trends are observed for all wood burning experiments during the period before the start of aging, implying slight but systematic differences between the loss rates of different OA species. These differences are likely
255 related to different volatility or size distribution of different species. Grieshop et al. (2009) reported bbPOA composition to be internally-mixed and size-independent, but the range in volatility of compounds in bbPOA may be responsible (~~2018b and Section S2~~Bertrand et al., 2018b and Supplement S2).

3.4 Aging by UV

In a UV experiment (experiment 4; Fig. 5b), as soon as the UV lights are turned on, several oxygenated fragment ions increase
260 in concentration, as expected based on around 20% mass formation observed; among those, CO_2^+ has the most prominent growth. When emissions are aged with UV lights, we observe positive values for the majority of AMS fragment concentrations and FTIR absorbances in the residual spectra, suggesting a significant formation of new oxidized species. Since bbPOA transformation was discussed in the previous section, we only consider the positive elements of the residual spectra here as an approximate representation of bbSOA and aged bbPOA. As can be seen from Fig. 6b, the normalized residual spectrum
265 in the UV experiments is mainly composed of CO_2^+ (and the fragments directly estimated from it: CO^+, H_2O^+, and OH^+), suggesting the abundance of carboxylic acids (Aiken et al., 2007). A few heavier mass fragments with two or more oxygen atoms (e.g., CHO_2^+, $C_2H_3O_2^+$, $C_4H_5O_2^+$, and $C_4H_3O_3^+$) have statistically non-zero values and can also be indicators of acids (Lambe et al., 2012) and polyfunctional organics (Fig. 6b). The sharp low-frequency carbonyl peak in the residual FTIR spectrum (1700 cm^{-1}) besides the broad OH peak of dimerized acids ($2400–3400 \text{ cm}^{-1}$) are other indicators of carboxylic acids in
270 the residual OA in the UV experiments (Fig. 7b). The latter, which is partially masked by the ammonium NH stretching peaks, becomes more prominent upon ammonium peak subtraction (~~Section S5~~Supplement S5). Although the relative contributions of bbSOA and oxidized bbPOA to the residual spectra are not clear, the formation of carboxylic acids via the oxidation of major wood burning VOCs and the abundance of carboxylic acids in the bbSOA is consistent with previous reports (Yazdani et al., 2021c; George et al., 2015; Chhabra et al., 2011). For certain atmospheric biomass burning samples, a unique FTIR spectral
275 profile with high abundance of carboxylic acids has been observed, resembling the aged bbOA (with UV) of this work (Section S6).

The wall-loss-corrected concentrations of some mass fragments decrease by more than 50% (Fig. 5b). Among the diminishing fragments, $C_9H_{11}O_3^+$, attributed to lignin-like compounds, and $C_2H_4O_2^+$, related to levoglucosan, decrease the most. Several non-oxygenated fragments with the $C_xH_y^+$ formula, related to hydrocarbons and aromatics, are also lost with aging

280 (e.g., $C_4H_9^+$, $C_5H_{11}^+$, $C_6H_6^+$, $C_8H_7^+$, and $C_8H_9^+$; Table 2). The extent of the decay for these species is significantly higher than what can be attributed to wall loss rate uncertainties shown in Table 2. There are also fragments (with single oxygen like $C_3H_4O^+$ or related to aromatics like $C_7H_7^+$) that increase in concentration briefly after the start of aging (around 30 min) and fall below their initial concentration with continued aging. These fragments might indicate the moderately oxygenated intermediate species or those that partition to the particle phase with increased OA loading but with a decay that becomes more

285 apparent with continued aging. The FTIR signatures of levoglucosan and lignin-like compounds also decrease significantly with the UV aging (Table 2), causing inverted peaks in the residual spectra (Fig. 7b). Locally inverted aCH peaks in the FTIR residual spectra of experiment 4 (Fig. 7b) support the hypothesis that hydrocarbons are lost with aging. The detectable decay of the aforementioned mentioned species is captured in both UV experiments 4 and 5 by both instruments (AMS and FTIR).

Gas-particle partitioning, heterogeneous ~~oxidant~~ oxidation reactions, and photolysis can play a role in the diminution of

290 the mentioned species in the particle phase. For semivolatile compounds like levoglucosan, particle-phase depletion can result from gas-phase losses and subsequent mass transfer from particles to gas. Bertrand et al. (2018b) proposed the prominent role of gas-particle partitioning and the subsequent vapor loss to the chamber walls for the depletion of levoglucosan in the particle phase. Comparing the trends of AMS levoglucosan-related fragments (particle phase) between reference and UV experiments of this work, however, the reaction of levoglucosan with the hydroxyl radical appears to be the dominant ~~factor for~~

295 ~~its depletion in the particle phase. For semi-volatile compounds like levoglucosan, particle-phase depletion can be the result of gas-phase depletion and the subsequent gas-particle partitioning. However~~ loss pathway. In contrast, the fast diminution of ~~fragments that are produced by~~ AMS fragments from less volatile species (e.g., heavy lignin-like compounds) highlights the role of particle-phase photolysis and heterogeneous reactions. In addition, a similar fast depletion of ~~$C_xH_y^+$ fragments~~ CxHy+ fragments in the particle phase merely due to heterogeneous reactions with the hydroxyl radical was also reported by George

300 et al. (2008).

The FTIR signature used for identification of lignin-like compounds in this work (sharp peak at 1515 cm^{-1}) has also been observed in the FTIR spectra of the HUmic LIke Substance (HULIS) isolated from aqueous extracts of atmospheric aerosols (Graber and Rudich, 2006). As discussed by Yazdani et al. (2021c), this peak can also be produced by small and relatively volatile molecules with a similar aromatic ring substitution to lignin (e.g., methoxyphenols and substituted syringols). The

305 $C_9H_{11}O_3^+$ and $C_{10}H_{13}O_3^+$ fragments in the AMS spectra might not be exclusive to non-volatile lignin and can be produced by smaller, more volatile molecules in bbOA resulting from lignin pyrolysis. There are, however, two observations that suggest the lignin-related fragments in this work can be attributed to compounds with a lower volatility than levoglucosan that exist predominantly in the particle phase under the conditions of the experiments (e.g., OA loading and temperature). First, the thermodenuder data suggest the lower volatility of compounds producing $C_9H_{11}O_3^+$ and $C_{10}H_{13}O_3^+$ ~~($C^\star$ estimated to be 1.83~~

310 ~~and 1.32 , respectively)~~ compared to species producing $C_2H_4O_2^+$ ~~($C^\star$ estimated to be 5.42 ;~~ Section S2). Second, the lower loss rate of $C_9H_{11}O_3^+$ in the absence of oxidants compared to other fragments including $C_2H_4O_2^+$ (Section S2) suggests the lower volatility of the corresponding species in that their concentration is mainly affected by particle-phase wall losses compared to particle- and gas-phase wall losses for levoglucosan.

Between the two marker fragments attributed to lignin-like compounds, $C_{10}H_{13}O_3^+$ and $C_9H_{11}O_3^+$, the former is a a heavier and less abundant fragment (Li et al., 2012), and appears to be more stable with regard to aging with its loss rate being one-third of that of the latter (Section S7). Because of this difference in decay rates, the ratio of $C_{10}H_{13}O_3^+$ to $C_9H_{11}O_3^+$ can potentially be used as an aging clock of atmospheric bbOA and warrants further study.

In these UV aging experiments, transformation of 10–17% of total bbPOA mass is estimated from the negative AMS residuals. The bbPOA transformation is estimated to be around 40% more intense for experiment 4 compared to experiment 5, consistent with the higher average OH concentration for the former (Table 1). The values of bbPOA transformation obtained with the AMS should be considered as a lower bound estimate for the chemical processing of primary bbPOA. This is because the increase in the concentration of some mass fragments owing to SOA condensation might outweigh the decay for the same fragments generated by bbPOA oxidation or evaporation. This can especially render the loss of small oxygenated fragments that are common to several species (Yazdani et al., 2021b) undetectable by the method. For instance in experiment 4, levoglucosan-marker fragments, $C_2H_4O_2^+$, and $C_3H_5O_2^+$, decrease the most with aging. Unlike these fragments, CHO^+, which is also produced in comparable amounts by levoglucosan fragmentation (Schneider et al., 2006), increases in concentration during the course of aging due to SOA condensation. By quantifying the inverted aliphatic CH, lignin, and levoglucosan peaks in the FTIR residual spectrum of this experiment (Fig. 7b) (representing the molecular structure of lignin by syringaldehyde), we estimate around 35 % (against 15 % estimated with AMS) of the POA mass to transform with aging.

We note that the change in composition with aging is not necessarily accompanied by a change in overall OA mass. For instance, in experiment 4, the wall-loss corrected OA mass concentration reaches a constant level about 1 h after the start of aging; while f_{44}-f_{43} ratios for the total and residual OAs gradually increase and the wall loss corrected organic carbon (OC) gradually decreases until the end of experiment (Section S8). The net loss of carbon from the particle phase and increased oxidation of the OA without an increase in its mass suggests that heterogeneous OH reactions and fragmentation are important mechanisms.

3.5 Aging under dark conditions

When emissions are Emissions aged in dark conditions in both dry and humid (experiments 6 and 8; Fig. 5c and d), the CO_2^+ fragment has OA enhancement is similar to that reported by Kodros et al. (2020). We observe the highest increase in the CO_2^+ fragment abundance. The average of the difference in residual spectra of wood and pellet burning is reported in Figs. 6c and d (differences among aging trajectories between fuel types are not substantial, as previously stated). In the residual FTIR spectra, higher abundance of the aCOH group relative to UV experiments is observed (7c–d). The formation of organic nitrates is also confirmed in the residual FTIR spectra (Fig. 7c–d) as well as with AMS. When emissions are aged in dry conditions, CHO^+ and $C_2H_3O^+$ are among the most prominent fragments in the residual spectra (besides CO_2^+) (Fig. 6c). This observation suggests the abundance of non-acid oxygenated species in the SOA formed by the nitrate radical. Some heavier mass fragments with a single oxygen atom (e.g., $C_3H_3O^+$ and $C_3H_5O^+$) are also observed in the average residual spectrum, supporting this hypothesis (Fig. 6c). Apart from the oxygenated mass fragments, high abundances of light $C_xH_y^+$ fragments (CH_3^+, and $C_3H_3^+$) are

observed in the residual AMS spectrum. When aged in humid conditions, the average residual AMS mass spectrum (Fig. 7d) is fairly similar to that of UV experiments (Fig. 7b).

Similar to the UV experiments, several mass fragments decrease more than what can be attributed to wall losses, but the mass fragments related to levoglucosan fragmentation do not diminish beyond that observed for the reference case. Under dry conditions, the majority of the diminishing fragments are in the $C_xH_y^+$ form or those related to lignin-like compounds (Fig. 5d). Under humid conditions, we observe that lignin-related fragments decay more prominently in the humid compared to the dry conditions (Table 2). The decreasing trend for the levoglucosan-related fragments starts before the initiation of aging (injection of ozone into the chamber) and it is not affected by it (Fig. 5d). This observation suggests that the dark aging is not responsible for the decay of levoglucosan. In this case, other factors such as acid catalyzed levoglucosan reactions in the aqueous phase (Holmes and Petrucci, 2006) or a more efficient removal of gas-phase levoglucosan by chamber walls might play a role. Similar diminution of hydrocarbons, anhydrosugars, and lignin-like compounds is observed in the the FTIR spectra of experiment 8 (Table 2 and Fig. 5d). Nighttime aging under dry conditions of our experiments result in a negligible bbPOA transformation, close to what is observed in the reference experiments (approximate 2%). Nighttime aging in humid conditions of our experiments, however, results in a slightly higher bbPOA transformation (up to 5%).

4 Conclusions

In this work, we characterized the evolution of bbPOA with aging using AMS and FTIR. The similarity of AMS and FTIR spectra of oxidized bbOA in the chamber — especially when aged with UV or in dark and humid conditions — to those of oxidized atmospheric OA contextualizes the extent of aging in these chamber experiments and underscores the relevance of these conclusions to aging under ambient conditions. Similarity was assessed by f43:f44 plots, PCA, and functional group composition — e.g., high concentration of carboxylic acids was observed in the UV-aged chamber bbOA are similar to what is observed in atmospheric bbOA samples. The aged fraction of bbOA in the chamber became more oxidized with continued aging. In certain cases, oxidation happened without a substantial increase in the bbOA mass concentration (and with a decrease in the OC mass concentration), highlighting the role of heterogeneous reactions and photolysis.

Based on AMS fragments exhibiting a net negative change, we conservatively estimated the transformation (due to oxidation and evaporation) of bbPOA mass to be 2–5% under nighttime aging conditions, and up to 17% of bbPOA with less than a day of atmospheric aging with UV. This latter amount was calculated to be twice as high with FTIR, based on absorptivities for aliphatic CH functional groups and signature peaks of levoglucosan and syringaldehyde (representing lignin-like compounds). The absorptivity-based approach considers mass transformations on a molecular rather than molecular fragment basis, and may be more relevant according to the representation of OA used in numerical models.

Biomass burning markers such as lignin-like compounds and anhydrosugars, as well as hydrocarbons were among the bbPOA compounds that degraded the most in the particle phase with aging (from 10 to 50% of original mass concentrations; up to six times greater than in reference experiments) according to both the AMS and FTIR. Unlike hydrocarbons and lignin-like compounds that degraded during both day- and night-time oxidation, anhydrosugars were observed to degrade effectively

only during the day-time oxidation. In addition, high humidity was observed to increase the loss rate of anhydrosugars in the particle phase. Since the degradation occurs for semi-volatile (levoglucosan) and less volatile (heavy lignin-like) compounds, gas-particle partitioning and heterogeneous reactions likely play a role. Different biomass burning-related fragments in the AMS spectra were observed to have different decay rates. These rate differences can potentially be used to identify the age of atmospheric bbOA, as well as the relative contribution of different aging mechanisms, provided that fragment ratios of anhyydrosugar and lignin-like compound in various emission sources can be better constratined.

Author contributions. AN, SNP, ST, and AY conceived the project. AY prepared filter sampling set-up. JKK, MP, KF, MM, SS performed the chamber experiments. KF processed AMS row signals. AY processed FTIR spectra and performed the data analysis, and wrote the manuscript. ST, AN, and SNP provided regular input on the analysis and the further editing of the manuscript. ST and AN provided overall supervision of the project.

Competing interests. We declare that no competing interests are present

Acknowledgements. This work was supported by the project PyroTRACH (ERC-2016-COG) funded from H2020-EU.1.1. - Excellent Science - European Research Council (ERC), project ID 726165 and funding from the Swiss National Science Foundation (200021_172923). SNP also acknowledges funding from the CHEVOPIN project of the Hellenic Foundation for Research & Innovation.

References

Abdi, H. and Williams, L. J.: Principal Component Analysis, Wiley Interdiscip. Rev. Comput. Stat., 2, 433–459, https://doi.org/10.1002/wics.101, 2010.

Aiken, A. C., DeCarlo, P. F., and Jimenez, J. L.: Elemental Analysis of Organic Species with Electron Ionization High-Resolution Mass Spectrometry, Anal. Chem., 79, 8350–8358, https://doi.org/10.1021/ac071150w, 2007.

Aiken, A. C., Salcedo, D., Cubison, M. J., Huffman, J. A., DeCarlo, P. F., Ulbrich, I. M., Docherty, K. S., Sueper, D., Kimmel, J. R., Worsnop, D. R., Trimborn, A., Northway, M., Stone, E. A., Schauer, J. J., Volkamer, R. M., Fortner, E., de Foy, B., Wang, J., Laskin, A., Shutthanandan, V., Zheng, J., Zhang, R., Gaffney, J., Marley, N. A., Paredes-Miranda, G., Arnott, W. P., Molina, L. T., Sosa, G., and Jimenez, J. L.: Mexico City Aerosol Analysis during MILAGRO Using High Resolution Aerosol Mass Spectrometry at the Urban Supersite (T0) – Part 1: Fine Particle Composition and Organic Source Apportionment, Atmos. Chem. Phys., p. 21, 2009.

Alves, C., Gonçalves, C., Fernandes, A. P., Tarelho, L., and Pio, C.: Fireplace and Woodstove Fine Particle Emissions from Combustion of Western Mediterranean Wood Types, Atmos. Res., 101, 692–700, https://doi.org/10.1016/j.atmosres.2011.04.015, 2011.

Bäfver, L. S., Leckner, B., Tullin, C., and Berntsen, M.: Particle Emissions from Pellets Stoves and Modern and Old-Type Wood Stoves, Biomass Bioenergy, 35, 3648–3655, https://doi.org/10.1016/j.biombioe.2011.05.027, 2011.

Barmet, P., Dommen, J., DeCarlo, P. F., Tritscher, T., Praplan, A. P., Platt, S. M., Prévôt, A. S. H., Donahue, N. M., and Baltensperger, U.: OH Clock Determination by Proton Transfer Reaction Mass Spectrometry at an Environmental Chamber, Atmos. Meas. Tech., 5, 647–656, https://doi.org/10.5194/amt-5-647-2012, 2012.

Bateman, A. P., Nizkorodov, S. A., Laskin, J., and Laskin, A.: Photolytic Processing of Secondary Organic Aerosols Dissolved in Cloud Droplets, Physical Chemistry Chemical Physics, 13, 12 199–12 212, https://doi.org/10.1039/C1CP20526A, 2011.

Bertrand, A., Stefenelli, G., Bruns, E. A., Pieber, S. M., Temime-Roussel, B., Slowik, J. G., Prévôt, A. S. H., Wortham, H., El Haddad, I., and Marchand, N.: Primary Emissions and Secondary Aerosol Production Potential from Woodstoves for Residential Heating: Influence of the Stove Technology and Combustion Efficiency, Atmos. Environ., 169, 65–79, https://doi.org/10.1016/j.atmosenv.2017.09.005, 2017.

Bertrand, A., Stefenelli, G., Jen, C. N., Pieber, S. M., Bruns, E. A., Ni, H., Temime-Roussel, B., Slowik, J. G., Goldstein, A. H., Haddad, I. E., Baltensperger, U., Prévôt, A. S. H., Wortham, H., and Marchand, N.: Evolution of the Chemical Fingerprint of Biomass Burning Organic Aerosol during Aging, Atmos. Chem. Phys., 18, 7607–7624, https://doi.org/10.5194/acp-18-7607-2018, 2018a.

Bertrand, A., Stefenelli, G., Pieber, S. M., Bruns, E. A., Temime-Roussel, B., Slowik, J. G., Wortham, H., Prévôt, A. S. H., Haddad, I. E., and Marchand, N.: Influence of the Vapor Wall Loss on the Degradation Rate Constants in Chamber Experiments of Levoglucosan and Other Biomass Burning Markers, Atmos. Chem. Phys., 18, 10 915–10 930, https://doi.org/10.5194/acp-18-10915-2018, 2018b.

Bond, T. C., Doherty, S. J., Fahey, D. W., Forster, P. M., Berntsen, T., DeAngelo, B. J., Flanner, M. G., Ghan, S., Kärcher, B., Koch, D., Kinne, S., Kondo, Y., Quinn, P. K., Sarofim, M. C., Schultz, M. G., Schulz, M., Venkataraman, C., Zhang, H., Zhang, S., Bellouin, N., Guttikunda, S. K., Hopke, P. K., Jacobson, M. Z., Kaiser, J. W., Klimont, Z., Lohmann, U., Schwarz, J. P., Shindell, D., Storelvmo, T., Warren, S. G., and Zender, C. S.: Bounding the Role of Black Carbon in the Climate System: A Scientific Assessment, Journal of Geophysical Research: Atmospheres, 118, 5380–5552, https://doi.org/10.1002/jgrd.50171, 2013.

Boris, A. J., Takahama, S., Weakley, A. T., Debus, B. M., Fredrickson, C. D., Esparza-Sanchez, M., Burki, C., Reggente, M., Shaw, S. L., Edgerton, E. S., and Dillner, A. M.: Quantifying Organic Matter and Functional Groups in Particulate Matter Filter Samples from the Southeastern United States – Part 1: Methods, Atmos. Meas. Tech., 12, 5391–5415, https://doi.org/10.5194/amt-12-5391-2019, 2019.

Bruns, E., Krapf, M., Orasche, J., Huang, Y., Zimmermann, R., Drinovec, L., Močnik, G., El-Haddad, I., G. Slowik, J., Dommen, J., Baltensperger, U., and Prevot, A.: Characterization of Primary and Secondary Wood Combustion Products Generated under Different Burner Loads, Atmos. Chem. Phys., 15, 2825–2841, https://doi.org/10.5194/acp-15-2825-2015, 2015.

Burnett, R., Chen, H., Szyszkowicz, M., Fann, N., Hubbell, B., Pope, C. A., Apte, J. S., Brauer, M., Cohen, A., Weichenthal, S., Coggins, J., Di, Q., Brunekreef, B., Frostad, J., Lim, S. S., Kan, H., Walker, K. D., Thurston, G. D., Hayes, R. B., Lim, C. C., Turner, M. C., Jerrett, M., Krewski, D., Gapstur, S. M., Diver, W. R., Ostro, B., Goldberg, D., Crouse, D. L., Martin, R. V., Peters, P., Pinault, L., Tjepkema, M., van Donkelaar, A., Villeneuve, P. J., Miller, A. B., Yin, P., Zhou, M., Wang, L., Janssen, N. A. H., Marra, M., Atkinson, R. W., Tsang, H., Thach, T. Q., Cannon, J. B., Allen, R. T., Hart, J. E., Laden, F., Cesaroni, G., Forastiere, F., Weinmayr, G., Jaensch, A., Nagel, G., Concin, H., and Spadaro, J. V.: Global Estimates of Mortality Associated with Long-Term Exposure to Outdoor Fine Particulate Matter, PNAS, 115, 9592–9597, https://doi.org/10.1073/pnas.1803222115, 2018.

Canagaratna, M. R., Jayne, J. T., Jimenez, J. L., Allan, J. D., Alfarra, M. R., Zhang, Q., Onasch, T. B., Drewnick, F., Coe, H., Middlebrook, A., Delia, A., Williams, L. R., Trimborn, A. M., Northway, M. J., DeCarlo, P. F., Kolb, C. E., Davidovits, P., and Worsnop, D. R.: Chemical and Microphysical Characterization of Ambient Aerosols with the Aerodyne Aerosol Mass Spectrometer, Mass Spectrom. Rev., 26, 185–222, https://doi.org/10.1002/mas.20115, 2007.

Canagaratna, M. R., Jimenez, J. L., Kroll, J. H., Chen, Q., Kessler, S. H., Massoli, P., Hildebrandt Ruiz, L., Fortner, E., Williams, L. R., Wilson, K. R., Surratt, J. D., Donahue, N. M., Jayne, J. T., and Worsnop, D. R.: Elemental Ratio Measurements of Organic Compounds Using Aerosol Mass Spectrometry: Characterization, Improved Calibration, and Implications, Atmos. Chem. Phys., 15, 253–272, https://doi.org/10.5194/acp-15-253-2015, 2015.

Chhabra, P. S., Ng, N. L., Canagaratna, M. R., Corrigan, A. L., Russell, L. M., Worsnop, D. R., Flagan, R. C., and Seinfeld, J. H.: Elemental Composition and Oxidation of Chamber Organic Aerosol, Atmos. Chem. Phys., 11, 8827–8845, https://doi.org/10.5194/acp-11-8827-2011, 2011.

Coury, C. and Dillner, A. M.: A Method to Quantify Organic Functional Groups and Inorganic Compounds in Ambient Aerosols Using Attenuated Total Reflectance FTIR Spectroscopy and Multivariate Chemometric Techniques, Atmos. Environ., 42, 5923–5932, https://doi.org/10.1016/j.atmosenv.2008.03.026, 2008.

Donahue, N. M., Robinson, A. L., Stanier, C. O., and Pandis, S. N.: Coupled Partitioning, Dilution, and Chemical Aging of Semivolatile Organics, Environ. Sci. Technol., 40, 2635–2643, https://doi.org/10.1021/es052297c, 2006.

Donahue, N. M., Henry, K. M., Mentel, T. F., Kiendler-Scharr, A., Spindler, C., Bohn, B., Brauers, T., Dorn, H. P., Fuchs, H., Tillmann, R., Wahner, A., Saathoff, H., Naumann, K.-H., Möhler, O., Leisner, T., Müller, L., Reinnig, M.-C., Hoffmann, T., Salo, K., Hallquist, M., Frosch, M., Bilde, M., Tritscher, T., Barmet, P., Praplan, A. P., DeCarlo, P. F., Dommen, J., Prévôt, A. S. H., and Baltensperger, U.: Aging of Biogenic Secondary Organic Aerosol via Gas-Phase OH Radical Reactions, PNAS, 109, 13 503–13 508, https://doi.org/10.1073/pnas.1115186109, 2012.

Faber, P., Drewnick, F., Bierl, R., and Borrmann, S.: Complementary Online Aerosol Mass Spectrometry and Offline FT-IR Spectroscopy Measurements: Prospects and Challenges for the Analysis of Anthropogenic Aerosol Particle Emissions, Atmos. Environ., 166, 92–98, https://doi.org/10.1016/j.atmosenv.2017.07.014, 2017.

Farmer, D. K., Matsunaga, A., Docherty, K. S., Surratt, J. D., Seinfeld, J. H., Ziemann, P. J., and Jimenez, J. L.: Response of an Aerosol Mass Spectrometer to Organonitrates and Organosulfates and Implications for Atmospheric Chemistry, PNAS, 107, 6670–6675, https://doi.org/10.1073/pnas.0912340107, 2010.

Fine, P. M., Cass, G. R., and Simoneit, B. R. T.: Chemical Characterization of Fine Particle Emissions from the Fireplace Combustion of Woods Grown in the Southern United States, Environ. Sci. Technol., 36, 1442–1451, https://doi.org/10.1021/es0108988, 2002.

470 Ford, B., Martin, M. V., Zelasky, S. E., Fischer, E. V., Anenberg, S. C., Heald, C. L., and Pierce, J. R.: Future Fire Impacts on Smoke Concentrations, Visibility, and Health in the Contiguous United States, GeoHealth, 2, 229–247, https://doi.org/10.1029/2018GH000144, 2018.

George, I. J., Slowik, J., and Abbatt, J. P. D.: Chemical Aging of Ambient Organic Aerosol from Heterogeneous Reaction with Hydroxyl Radicals, Geophys. Res. Lett., 35, L13 811, https://doi.org/10.1029/2008GL033884, 2008.

475 George, K. M., Ruthenburg, T. C., Smith, J., Yu, L., Zhang, Q., Anastasio, C., and Dillner, A. M.: FT-IR Quantification of the Carbonyl Functional Group in Aqueous-Phase Secondary Organic Aerosol from Phenols, Atmos. Environ., 100, 230–237, https://doi.org/10.1016/j.atmosenv.2014.11.011, 2015.

Gkatzelis, G. I., Papanastasiou, D. K., Florou, K., Kaltsonoudis, C., Louvaris, E., and Pandis, S. N.: Measurement of nonvolatile particle number size distribution, Atmospheric Measurement Techniques, 9, 103–114, https://doi.org/10.5194/amt-9-103-2016, 2016.

480 Graber, E. R. and Rudich, Y.: Atmospheric HULIS: How Humic-like Are They? A Comprehensive and Critical Review, Atmos. Chem. Phys., 6, 729–753, https://doi.org/10.5194/acp-6-729-2006, 2006.

Grieshop, A. P., Donahue, N. M., and Robinson, A. L.: Laboratory Investigation of Photochemical Oxidation of Organic Aerosol from Wood Fires 2: Analysis of Aerosol Mass Spectrometer Data, Atmos. Chem. Phys., 9, 2227–2240, https://doi.org/10.5194/acp-9-2227-2009, 2009.

485 Hallquist, M., Wenger, J. C., Baltensperger, U., Rudich, Y., Simpson, D., Claeys, M., Dommen, J., Donahue, N. M., George, C., Goldstein, A. H., Hamilton, J. F., Herrmann, H., Hoffmann, T., Iinuma, Y., Jang, M., Jenkin, M. E., Jimenez, J. L., Kiendler-Scharr, A., Maenhaut, W., McFiggans, G., Mentel, T. F., Monod, A., Prévôt, A. S. H., Seinfeld, J. H., Surratt, J. D., Szmigielski, R., and Wildt, J.: The Formation, Properties and Impact of Secondary Organic Aerosol: Current and Emerging Issues, Atmos. Chem. Phys., 9, 5155–5236, https://doi.org/10.5194/acp-9-5155-2009, 2009.

490 Hearn, J. D., Lovett, A. J., and Smith, G. D.: Ozonolysis of Oleic Acid Particles: Evidence for a Surface Reaction and Secondary Reactions Involving Criegee Intermediates, Phys. Chem. Chem. Phys., 7, 501–511, https://doi.org/10.1039/B414472D, 2005.

Hennigan, C. J., Sullivan, A. P., Collett, J. L., and Robinson, A. L.: Levoglucosan Stability in Biomass Burning Particles Exposed to Hydroxyl Radicals, Geophys. Res. Lett., 37, L09 806, https://doi.org/10.1029/2010GL043088, 2010.

Hennigan, C. J., Miracolo, M. A., Engelhart, G. J., May, A. A., Presto, A. A., Lee, T., Sullivan, A. P., McMeeking, G. R., Coe, H., Wold,
495 C. E., Hao, W.-M., Gilman, J. B., Kuster, W. C., de Gouw, J., Schichtel, B. A., Collett, J. L. J., Kreidenweis, S. M., and Robinson, A. L.: Chemical and Physical Transformations of Organic Aerosol from the Photo-Oxidation of Open Biomass Burning Emissions in an Environmental Chamber, Atmospheric Chemistry and Physics, 11, 7669–7686, https://doi.org/10.5194/acp-11-7669-2011, 2011.

Henry, K. M. and Donahue, N. M.: Photochemical Aging of Alpha-Pinene Secondary Organic Aerosol: Effects of OH Radical Sources and Photolysis, J. Phys. Chem. A, 116, 5932–5940, https://doi.org/10.1021/jp210288s, 2012.

500 Holmes, B. J. and Petrucci, G. A.: Water-Soluble Oligomer Formation from Acid-Catalyzed Reactions of Levoglucosan in Proxies of Atmospheric Aqueous Aerosols, Environ. Sci. Technol., 40, 4983–4989, https://doi.org/10.1021/es060646c, 2006.

Hotelling, H.: Analysis of a Complex of Statistical Variables into Principal Components, J. Educ. Psychol., 24, 417–441, https://doi.org/10.1037/h0071325, 1933.

Hung, H.-M., Katrib, Y., and Martin, S. T.: Products and Mechanisms of the Reaction of Oleic Acid with Ozone and Nitrate Radical, The
505 Journal of Physical Chemistry A, 109, 4517–4530, https://doi.org/10.1021/jp0500900, 2005.

Johansson, L. S., Leckner, B., Gustavsson, L., Cooper, D., Tullin, C., and Potter, A.: Emission Characteristics of Modern and Old-Type Residential Boilers Fired with Wood Logs and Wood Pellets, Atmos. Environ., 38, 4183–4195, https://doi.org/10.1016/j.atmosenv.2004.04.020, 2004.

Jorga, S. D., Florou, K., Kaltsonoudis, C., Kodros, J. K., Vasilakopoulou, C., Cirtog, M., Fouqueau, A., Picquet-Varrault, B., Nenes, A., and Pandis, S. N.: Nighttime Chemistry of Biomass Burning Emissions in Urban Areas: A Dual Mobile Chamber Study, Atmos. Chem. Phys., 21, 15 337–15 349, https://doi.org/10.5194/acp-21-15337-2021, 2021.

Kalberer, M., Sax, M., and Samburova, V.: Molecular Size Evolution of Oligomers in Organic Aerosols Collected in Urban Atmospheres and Generated in a Smog Chamber, Environ. Sci. Technol., 40, 5917–5922, https://doi.org/10.1021/es0525760, 2006.

Kaltsonoudis, C., Kostenidou, E., Louvaris, E., Psichoudaki, M., Tsiligiannis, E., Florou, K., Liangou, A., and Pandis, S. N.: Characterization of Fresh and Aged Organic Aerosol Emissions from Meat Charbroiling, Atmos. Chem. Phys., 17, 7143–7155, https://doi.org/10.5194/acp-17-7143-2017, 2017.

Kanakidou, M., Seinfeld, J. H., Pandis, S. N., Barnes, I., Dentener, F. J., Facchini, M. C., Dingenen, R. V., Ervens, B., Nenes, A., Nielsen, C. J., Swietlicki, E., Putaud, J. P., Balkanski, Y., Fuzzi, S., Horth, J., Moortgat, G. K., Winterhalter, R., Myhre, C. E. L., Tsigaridis, K., Vignati, E., Stephanou, E. G., and Wilson, J.: Organic Aerosol and Global Climate Modelling: A Review, Atmos. Chem. Phys., p. 71, 2005.

Kodros, J. K., Papanastasiou, D. K., Paglione, M., Masiol, M., Squizzato, S., Florou, K., Skyllakou, K., Kaltsonoudis, C., Nenes, A., and Pandis, S. N.: Rapid Dark Aging of Biomass Burning as an Overlooked Source of Oxidized Organic Aerosol, PNAS, 117, 33 028–33 033, https://doi.org/10.1073/pnas.2010365117, 2020.

Kodros, J. K., Kaltsonoudis, C., Paglione, M., Florou, K., Jorga, S. D., Vasilakopoulou, C., Cirtog, M., Cazaunau, M., Picquet-Varrault, B., Nenes, A., and Pandis, S. N.: Secondary Aerosol Formation in Dark Aging Experiments of Biomass Burning Emissions, Manuscript in preparation, 2022.

Kumar, N. K., Corbin, J. C., Bruns, E. A., Massabó, D., Slowik, J. G., Drinovec, L., Močnik, G., Prati, P., Vlachou, A., Baltensperger, U., Gysel, M., El-Haddad, I., and Prévôt, A. S. H.: Production of Particulate Brown Carbon during Atmospheric Aging of Residential Wood-Burning Emissions, Atmos. Chem. Phys., 18, 17 843–17 861, https://doi.org/10.5194/acp-18-17843-2018, 2018.

Lambe, A. T., Onasch, T. B., Croasdale, D. R., Wright, J. P., Martin, A. T., Franklin, J. P., Massoli, P., Kroll, J. H., Canagaratna, M. R., Brune, W. H., Worsnop, D. R., and Davidovits, P.: Transitions from Functionalization to Fragmentation Reactions of Laboratory Secondary Aerosol (SOA) Generated from the OH Oxidation of Alkane Precursors, Environ. Sci. Technol., 46, 5430–5437, https://doi.org/10.1021/es300274t, 2012.

Lanz, V. A., Prévôt, A. S. H., Alfarra, M. R., Weimer, S., Mohr, C., DeCarlo, P. F., Gianini, M. F. D., Hueglin, C., Schneider, J., Favez, O., D'Anna, B., George, C., and Baltensperger, U.: Characterization of Aerosol Chemical Composition with Aerosol Mass Spectrometry in Central Europe: An Overview, Atmos. Chem. Phys., 10, 10 453–10 471, https://doi.org/10.5194/acp-10-10453-2010, 2010.

Lee, B. H., Kostenidou, E., Hildebrandt, L., Riipinen, I., Engelhart, G. J., Mohr, C., DeCarlo, P. F., Mihalopoulos, N., Prevot, A. S. H., Baltensperger, U., and Pandis, S. N.: Measurement of the ambient organic aerosol volatility distribution: application during the Finokalia Aerosol Measurement Experiment (FAME-2008), Atmospheric Chemistry and Physics, 10, 12 149–12 160, https://doi.org/10.5194/acp-10-12149-2010, publisher: Copernicus GmbH, 2010.

Li, Y. J., Yeung, J. W. T., Leung, T. P. I., Lau, A. P. S., and Chan, C. K.: Characterization of Organic Particles from Incense Burning Using an Aerodyne High-Resolution Time-of-Flight Aerosol Mass Spectrometer, Aerosol Sci. Tech., 46, 654–665, https://doi.org/10.1080/02786826.2011.653017, 2012.

Mabato, B. R. G., Lyu, Y., Ji, Y., Li, Y. J., Huang, D. D., Li, X., Nah, T., Lam, C. H., and Chan, C. K.: Aqueous secondary organic aerosol formation from the direct photosensitized oxidation of vanillin in the absence and presence of ammonium nitrate, Atmospheric Chemistry and Physics, 22, 273–293, https://doi.org/10.5194/acp-22-273-2022, publisher: Copernicus GmbH, 2022.

McFiggans, G., Coe, H., Burgess, R., Allan, J., Cubison, M., Alfarra, M. R., Saunders, R., Saiz-Lopez, A., Plane, J. M. C., Wevill, D., Carpenter, L., Rickard, A. R., and Monks, P. S.: Direct Evidence for Coastal Iodine Particles from Laminaria Macroalgae – Linkage to Emissions of Molecular Iodine, Atmos. Chem. Phys., 4, 701–713, https://doi.org/10.5194/acp-4-701-2004, 2004.

Nah, T., Kessler, S. H., Daumit, K. E., Kroll, J. H., Leone, S. R., and Wilson, K. R.: Influence of Molecular Structure and Chemical Functionality on the Heterogeneous OH-Initiated Oxidation of Unsaturated Organic Particles, J. Phys. Chem. A, 118, 4106–4119, https://doi.org/10.1021/jp502666g, 2014.

Ng, N. L., Canagaratna, M. R., Jimenez, J. L., Chhabra, P. S., Seinfeld, J. H., and Worsnop, D. R.: Changes in Organic Aerosol Composition with Aging Inferred from Aerosol Mass Spectra, Atmos. Chem. Phys., 11, 6465–6474, https://doi.org/10.5194/acp-11-6465-2011, 2011.

Pandey, K. K.: A Study of Chemical Structure of Soft and Hardwood and Wood Polymers by FTIR Spectroscopy, Journal of Applied Polymer Science, 71, 1969–1975, https://doi.org/10.1002/(SICI)1097-4628(19990321)71:12<1969::AID-APP6>3.0.CO;2-D, 1999.

Parks, D. A., Raj, K. V., Berry, C. A., Weakley, A. T., Griffiths, P. R., and Miller, A. L.: Towards a Field-Portable Real-Time Organic and Elemental Carbon Monitor, Mining, Metallurgy & Exploration, 36, 765–772, https://doi.org/10.1007/s42461-019-0064-8, 2019.

Pathak, R. K., Stanier, C. O., Donahue, N. M., and Pandis, S. N.: Ozonolysis of Alpha-Pinene at Atmospherically Relevant Concentrations: Temperature Dependence of Aerosol Mass Fractions (Yields), J. Geophys. Res.-Atmos., 112, https://doi.org/10.1029/2006JD007436, 2007.

Pope, C. A., Ezzati, M., and Dockery, D. W.: Fine-Particulate Air Pollution and Life Expectancy in the United States, N. Engl. J. Med., 360, 376–386, https://doi.org/10.1056/NEJMsa0805646, 2009.

Puxbaum, H., Caseiro, A., Sánchez-Ochoa, A., Kasper-Giebl, A., Claeys, M., Gelencsér, A., Legrand, M., Preunkert, S., and Pio, C.: Levoglucosan Levels at Background Sites in Europe for Assessing the Impact of Biomass Combustion on the European Aerosol Background, J. Geophys. Res.-Atmos., 112, D23S05, https://doi.org/10.1029/2006JD008114, 2007.

Qi, L., Chen, M., Stefenelli, G., Pospisilova, V., Tong, Y., Bertrand, A., Hueglin, C., Ge, X., Baltensperger, U., Prévôt, A. S. H., and Slowik, J. G.: Organic Aerosol Source Apportionment in Zurich Using an Extractive Electrospray Ionization Time-of-Flight Mass Spectrometer (EESI-TOF-MS) – Part 2: Biomass Burning Influences in Winter, Atmos. Chem. Phys., 19, 8037–8062, https://doi.org/10.5194/acp-19-8037-2019, 2019.

Reggente, M., Dillner, A. M., and Takahama, S.: Predicting Ambient Aerosol Thermal–Optical Reflectance (TOR) Measurements from Infrared Spectra: Extending the Predictions to Different Years and Different Sites, Atmos. Meas. Tech., 9, 441–454, https://doi.org/10.5194/amt-9-441-2016, 2016.

Reggente, M., Dillner, A. M., and Takahama, S.: Analysis of Functional Groups in Atmospheric Aerosols by Infrared Spectroscopy: Systematic Intercomparison of Calibration Methods for US Measurement Network Samples, Atmos. Meas. Tech., 12, 2287–2312, https://doi.org/10.5194/amt-12-2287-2019, 2019.

Robinson, A. L., Donahue, N. M., and Rogge, W. F.: Photochemical Oxidation and Changes in Molecular Composition of Organic Aerosol in the Regional Context, Journal of Geophysical Research: Atmospheres, 111, https://doi.org/10.1029/2005JD006265, 2006.

Robinson, A. L., Donahue, N. M., Shrivastava, M. K., Weitkamp, E. A., Sage, A. M., Grieshop, A. P., Lane, T. E., Pierce, J. R., and Pandis, S. N.: Rethinking Organic Aerosols: Semivolatile Emissions and Photochemical Aging, Science, 315, 1259–1262, https://doi.org/10.1126/science.1133061, 2007.

Russell, L. M.: Aerosol Organic-Mass-to-Organic- Carbon Ratio Measurements, Environ. Sci. Technol., 37, 2982–2987, https://doi.org/10.1021/es026123w, 2003.

Russo, C., Stanzione, F., Tregrossi, A., and Ciajolo, A.: Infrared Spectroscopy of Some Carbon-Based Materials Relevant in Combustion: Qualitative and Quantitative Analysis of Hydrogen, Carbon, 74, 127–138, https://doi.org/10.1016/j.carbon.2014.03.014, 2014.

Ruthenburg, T. C., Perlin, P. C., Liu, V., McDade, C. E., and Dillner, A. M.: Determination of Organic Matter and Organic Matter to Organic Carbon Ratios by Infrared Spectroscopy with Application to Selected Sites in the IMPROVE Network, Atmos. Environ., 86, 47–57, https://doi.org/10.1016/j.atmosenv.2013.12.034, 2014.

Schneider, J., Weimer, S., Drewnick, F., Borrmann, S., Helas, G., Gwaze, P., Schmid, O., Andreae, M. O., and Kirchner, U.: Mass Spectrometric Analysis and Aerodynamic Properties of Various Types of Combustion-Related Aerosol Particles, Int. J. Mass Spectrom., 258, 37–49, https://doi.org/10.1016/j.ijms.2006.07.008, 2006.

Seinfeld, J. H. and Pandis, S. N.: Atmospheric Chemistry and Physics: From Air Pollution to Climate Change, John Wiley & Sons, Hoboken, NJ, 2016.

Shiraiwa, M., Ueda, K., Pozzer, A., Lammel, G., Kampf, C. J., Fushimi, A., Enami, S., Arangio, A. M., Fröhlich-Nowoisky, J., Fujitani, Y., Furuyama, A., Lakey, P. S. J., Lelieveld, J., Lucas, K., Morino, Y., Pöschl, U., Takahama, S., Takami, A., Tong, H., Weber, B., Yoshino, A., and Sato, K.: Aerosol Health Effects from Molecular to Global Scales, Environ. Sci. Technol., 51, 13 545–13 567, https://doi.org/10.1021/acs.est.7b04417, 2017.

Slade, J. H. and Knopf, D. A.: Heterogeneous OH Oxidation of Biomass Burning Organic Aerosol Surrogate Compounds: Assessment of Volatilisation Products and the Role of OH Concentration on the Reactive Uptake Kinetics, Physical Chemistry Chemical Physics, 15, 5898–5915, https://doi.org/10.1039/C3CP44695F, 2013.

SpectraBase, John Wiley & Sons, Inc.: https://spectrabase.com/, last accessed 8/26/2022, 2022.

Takahama, S., Johnson, A., and Russell, L. M.: Quantification of Carboxylic and Carbonyl Functional Groups in Organic Aerosol Infrared Absorbance Spectra, Aerosol Sci. Tech., 47, 310–325, https://doi.org/10.1080/02786826.2012.752065, 2013.

Theodoritsi, G. N., Ciarelli, G., and Pandis, S. N.: Simulation of the Evolution of Biomass Burning Organic Aerosol with Different Volatility Basis Set Schemes in PMCAMx-SRv1.0, Geoscientific Model Development Discussions, pp. 1–33, https://doi.org/10.5194/gmd-2020-295, 2020.

Tiitta, P., Leskinen, A., Hao, L., Yli-Pirilä, P., Kortelainen, M., Grigonyte, J., Tissari, J., Lamberg, H., Hartikainen, A., Kuuspalo, K., Kortelainen, A.-M., Virtanen, A., Lehtinen, K. E. J., Komppula, M., Pieber, S., Prévôt, A. S. H., Onasch, T. B., Worsnop, D. R., Czech, H., Zimmermann, R., Jokiniemi, J., and Sippula, O.: Transformation of Logwood Combustion Emissions in a Smog Chamber: Formation of Secondary Organic Aerosol and Changes in the Primary Organic Aerosol upon Daytime and Nighttime Aging, Atmos. Chem. Phys., 16, 13 251–13 269, https://doi.org/10.5194/acp-16-13251-2016, 2016.

Tolbert, A. and Ragauskas, A. J.: Advances in Understanding the Surface Chemistry of Lignocellulosic Biomass via Time-of-Flight Secondary Ion Mass Spectrometry, Energy Sci. Eng., 5, 5–20, https://doi.org/10.1002/ese3.144, 2017.

Tsui, W. G. and McNeill, V. F.: Modeling Secondary Organic Aerosol Production from Photosensitized Humic-like Substances (HULIS), Environmental Science & Technology Letters, 5, 255–259, https://doi.org/10.1021/acs.estlett.8b00101, publisher: American Chemical Society, 2018.

Wang, N., Kostenidou, E., Donahue, N. M., and Pandis, S. N.: Multi-Generation Chemical Aging of Alpha-Pinene Ozonolysis Products by Reactions with OH, Atmospheric Chemistry and Physics, 18, 3589–3601, https://doi.org/10.5194/acp-18-3589-2018, 2018.

Wehner, B., Philippin, S., and Wiedensohler, A.: Design and calibration of a thermodenuder with an improved heating unit to measure the size-dependent volatile fraction of aerosol particles, Journal of Aerosol Science, 33, 1087–1093, https://doi.org/10.1016/S0021-8502(02)00056-3, 2002.

Yazdani, A.: Chemical characterization of organic aerosols with a focus on biomass burning and mid-infrared spectroscopy, Ph.D. thesis, École Polytechnique Fédérale de Lausanne, 2022.

Yazdani, A., Dillner, A. M., and Takahama, S.: Estimating Mean Molecular Weight, Carbon Number, and OM/OC with Mid-Infrared Spectroscopy in Organic Particulate Matter Samples from a Monitoring Network, Atmos. Meas. Tech., 14, 4805–4827, https://doi.org/10.5194/amt-14-4805-2021, 2021a.

Yazdani, A., Dudani, N., El Haddad, I., Bertrand, A., Prévôt, A. S. H., and Dillner, A. M.: Fragment Ion-Functional Group Relationships in Organic Aerosols Using Aerosol Mass Spectrometry and Mid-Infrared Spectroscopy, Atmos. Meas. Tech. Discuss. [preprint], https://doi.org/10.5194/amt-2021-186, 2021b.

Yazdani, A., Dudani, N., Takahama, S., Bertrand, A., Prévôt, A. S. H., El Haddad, I., and Dillner, A. M.: Characterization of Primary and Aged Wood Burning and Coal Combustion Organic Aerosols in Environmental Chamber and Its Implications for Atmospheric Aerosols, Atmos. Chem. Phys., 21, 10 273–10 293, https://doi.org/10.5194/acp-21-10273-2021, 2021c.

Zhang, Q., Jimenez, J. L., Canagaratna, M. R., Allan, J. D., Coe, H., Ulbrich, I., Alfarra, M. R., Takami, A., Middlebrook, A. M., Sun, Y. L., Dzepina, K., Dunlea, E., Docherty, K., DeCarlo, P. F., Salcedo, D., Onasch, T., Jayne, J. T., Miyoshi, T., Shimono, A., Hatakeyama, S., Takegawa, N., Kondo, Y., Schneider, J., Drewnick, F., Borrmann, S., Weimer, S., Demerjian, K., Williams, P., Bower, K., Bahreini, R., Cottrell, L., Griffin, R. J., Rautiainen, J., Sun, J. Y., Zhang, Y. M., and Worsnop, D. R.: Ubiquity and Dominance of Oxygenated Species in Organic Aerosols in Anthropogenically-Influenced Northern Hemisphere Midlatitudes, Geophys. Res. Lett., 34, https://doi.org/10.1029/2007GL029979, 2007.

Zhang, R., Gen, M., Liang, Z., Li, Y. J., and Chan, C. K.: Photochemical Reactions of Glyoxal during Particulate Ammonium Nitrate Photolysis: Brown Carbon Formation, Enhanced Glyoxal Decay, and Organic Phase Formation, Environmental Science & Technology, 56, 1605–1614, https://doi.org/10.1021/acs.est.1c07211, publisher: American Chemical Society, 2022.

Tables

Table 1. Description of experiments and initial O_3 and NO_2 concentrations.

Experiment	Type	Fuel	NO_2 (ppb)	O_3 (ppb)	RH (%)	OH (molecule cm^{-3})
1	Reference (no oxidant)	Wood	–	–	10	–
2	Reference (no oxidant)	Pellet	–	–	10	–
3	Reference (no oxidant)	Wood	–	–	50	–
4	UV + 30 pbb SO_2	Wood	–	–	50	5.0×10^6
5	UV + 80 pbb SO_2	Wood	–	–	50	3.0×10^6
6	Dark and dry	Wood	100	100	10	–
7	Dark and dry	Pellet	100	100	10	–
8	Dark and humid	Wood	100	100	80	–
9	Dark and humid	Pellet	100	100	60	–

Table 2. Summary of wall loss rates, and the ratio of the bbPOA concentration and certain markers in the aged bbOA to those in fresh bbOA.

	Reference (no oxidant)			UV		Dark and dry		Dark and humid	
	Exp. 1	Exp. 2	Exp. 3	Exp. 4	Exp. 5	Exp. 6[b]	Exp. 7	Exp. 8	Exp. 9
k_{OA} (h^{-1})	0.06±12%[c]	0.06±11%	0.08±10%	0.10±6%	0.10±8%	0.07±10%	0.09 ±10%	0.11±5%	0.10±7%
bbPOA FTIR	0.88	0.85	0.70	–	–	–	–	–	–
bbPOA AMS	0.90	0.85	0.73	0.63	0.68	0.77	0.73	0.64	0.68
Levoglucosan FTIR	0.88	0.83	0.54	0.27	0.40	–	0.88	0.35	0.65
$C_2H_4O_2^+$	0.88	0.91	0.52	0.27	0.36	0.90	0.78	0.40	0.54
$C_3H_5O_2^+$	0.96	0.91	0.67	0.36	0.45	0.90	0.79	0.51	0.58
Lignin FTIR	1.01	0.83	0.84	0.10	0.24	–	0.89	0.34	0.10
$C_8H_9O_2^+$	0.94	0.79	0.73	0.13	0.18	0.65	0.69	0.20	0.25
$C_9H_{11}O_3^+$	0.95	0.70	0.78	0.10	0.11	0.53	0.68	0.18	0.50
$C_{10}H_{13}O_3^+$	0.94	0.82	0.77	0.40	0.56	0.90	0.72	0.48	0.50
aCH FTIR[a]	>1	>1	>1	0.50	0.45	–	0.45	>1	>1
$C_4H_9^+$	0.91	0.83	0.75	0.35	0.38	0.75	0.60	0.59	0.50
$C_5H_{11}^+$	0.90	0.84	0.75	0.35	0.48	0.80	0.55	0.60	0.52

[a] Approximate values by which FTIR bbPOA spectra should be scaled to avoid inverted local CH peaks when subtracting from aged OA spectra.

[b] FTIR measurements were discarded for experiment 6 due to the unusually low bbOA mass sampled on the filter.

[c] Uncertainties are based on 90 % confidence interval.

Figures
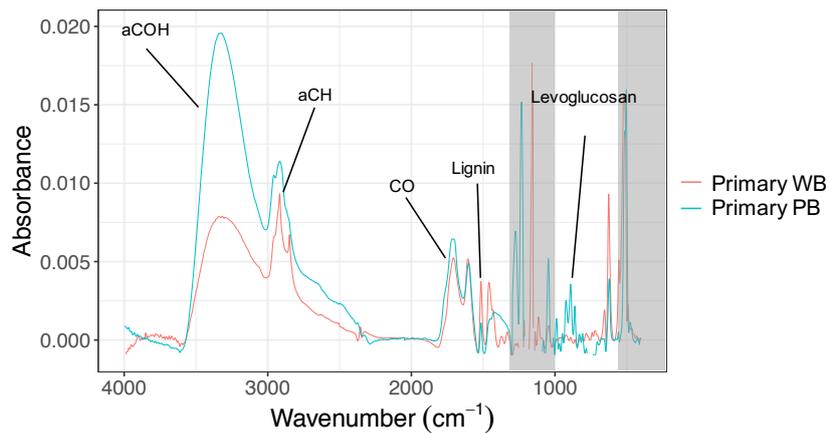
Figure 1. FTIR spectra of primary wood burning (WB) and pellet burning (PB) aerosols of experiment 6 and 7, respectively. Important functional groups or biomass burning markers are indicated. Regions with strong interferences from the collection substrate are shaded in gray.
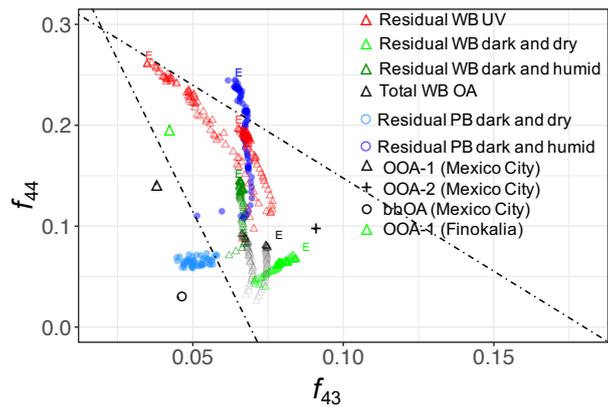
Figure 2. Aging trajectories of wood burning (WB) and pellet burning (PB) aerosols in the chamber with UV lights and dark aging ~~shown~~ in f_{44}-f_{43} ($f_{CO_2^+}$-$f_{C_2H_3O^+}$) plot. Finokalia ~~OOA~~ OOA-1 is obtained from Florou (*manuscript in preparation*, ~~2022~~2023). End of trajectories are shown with letter E.
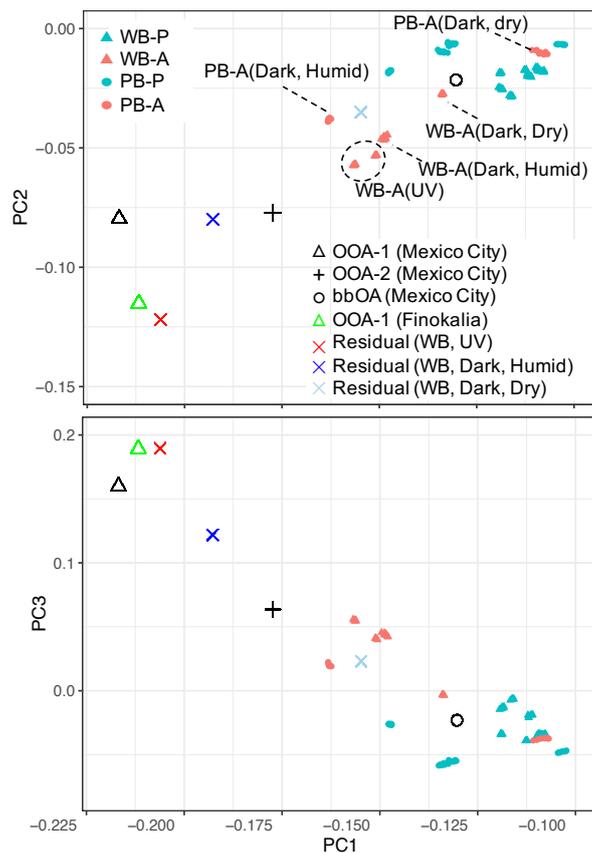
Figure 3. PC1-PC2 and PC1-PC3 biplots for primary, aged, and residual bbOA. WB-P (wood burning, primary), WB-A (wood burning, primary), PB-P (pellet burning, primary), PB-A (pellet burning, aged), and ambient aerosols from Mexico City and Finokalia are raw bbOA spectra (no estimation of residual spectra). Finokalia OOA-1 is obtained from Florou (*manuscript in preparation*, ~~2022~~2023) and Mexico City OOA-1, 2, and bbOA from Aiken et al. (2009).
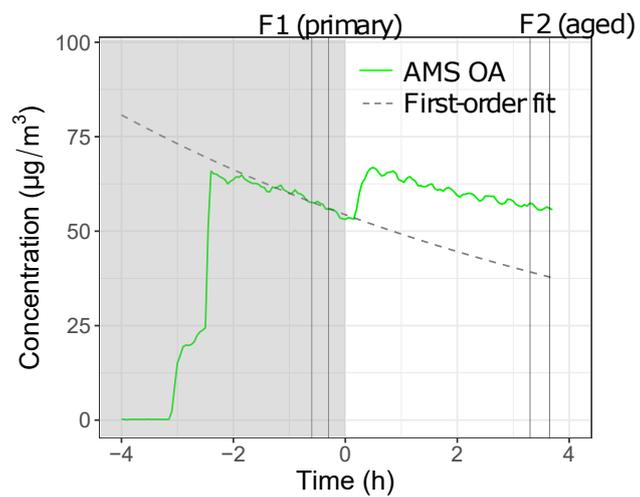
Figure 4. The AMS OA and apparent POA concentrations using a first-order wall loss for experiment 5. Dark and light regions of the figure indicate periods before and after switching on UV lights. Vertical lines indicate the periods of filter sampling for primary and aged aerosols.
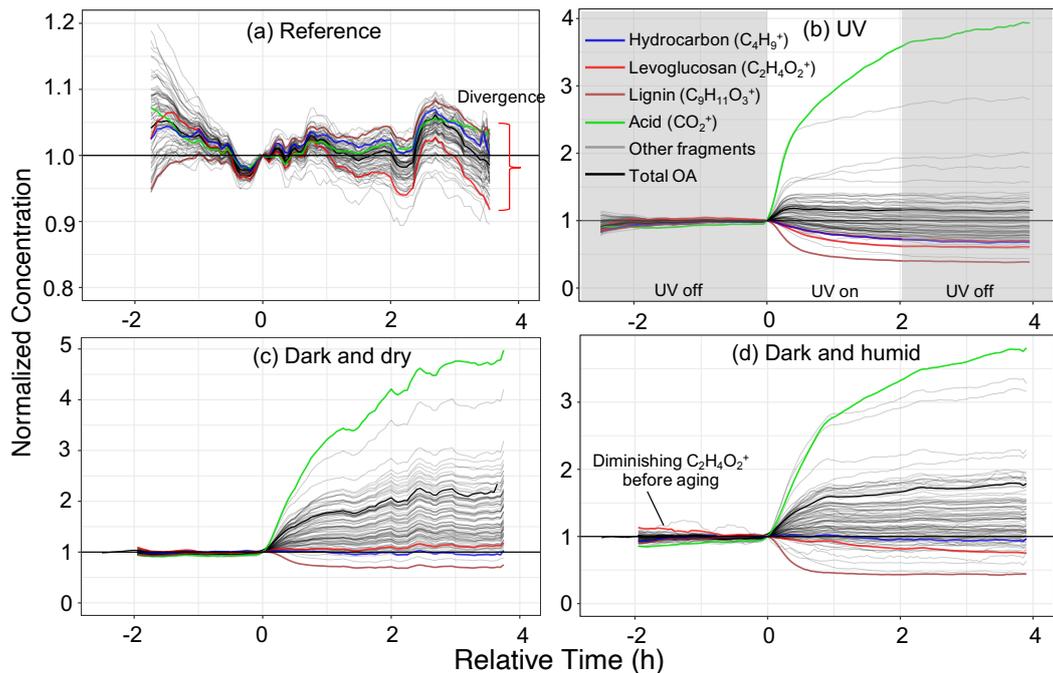
Figure 5. Time series of wall-loss-corrected and normalized concentrations of individual mass fragments in different aging scenarios. Only mass fragments contributing more than 0.25 % to the total OA mass concentration are shown. Fragments attributed to different species are shown in color. Panels a–d represent experiments 1, 4, 6, and 8, respectively. Time zero indicates the initiation of aging.
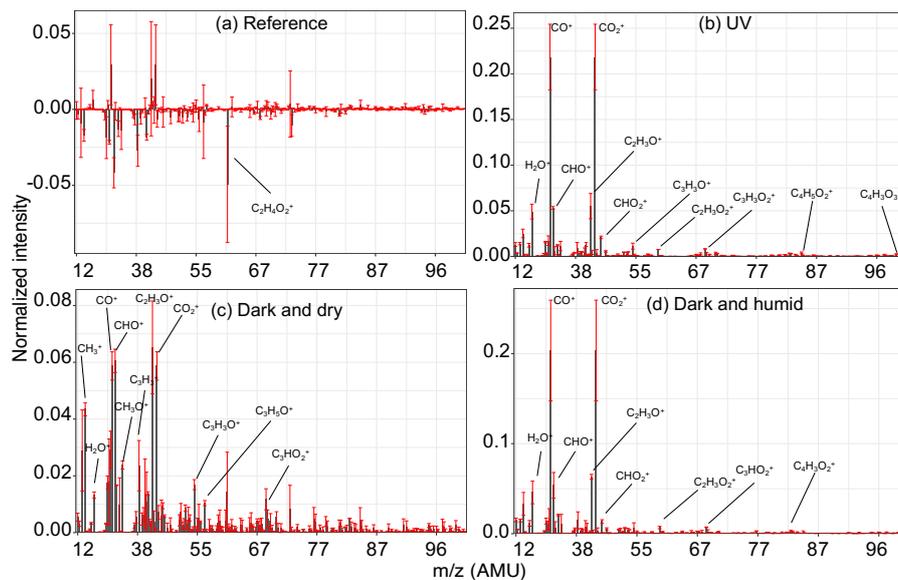
Figure 6. Residual AMS spectra of bbOA (normalized) for different aging experiments. Spectra are averaged over experiments of the same category and error bars show the range for each category.
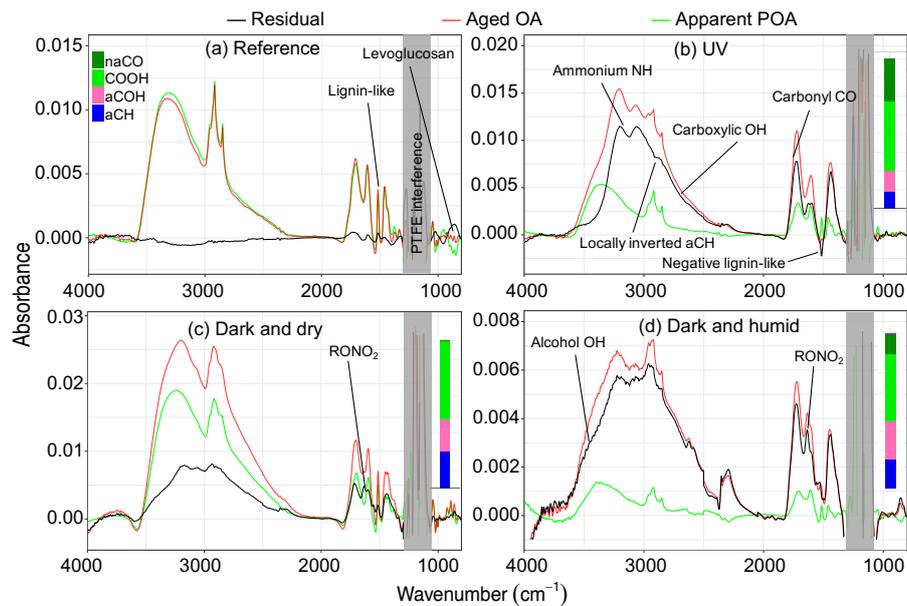
Figure 7. FTIR spectra of aged aerosols (red), their apparent primary fraction (green), and the residual aerosols (black) for different aging experiments. Panels a–d represent Exp. 1, 4, 7, and 8, respectively. Normalized functional group compositions from peak fitting is shown for the residual spectra. Ammonium subtracted spectra for panels b and c are shown in supplement Fig. S6S6.

Supplement for "Chemical evolution of primary and secondary biomass burning aerosols during daytime and nighttime"

Amir Yazdani[1], Satoshi Takahama[1], John K. Kodros[2], Marco Paglione[2,3], Mauro Masiol[2], Stefania Squizzato[2], Kalliopi Florou[2], Christos Kaltsonoudis[2], Spiro D. Jorga[2], Spyros N. Pandis[2,4], and Athanasios Nenes[1,2]

[1]Laboratory of atmospheric processes and their impacts (LAPI), ENAC/IIE, Ecole polytechnique fédérale de Lausanne (EPFL), Lausanne, Switzerland
[2]Institute for Chemical Engineering Sciences, Foundation for Research and Technology Hellas (ICE-HT/FORTH), Patra, Greece
[3]Italian National Research Council - Institute of Atmospheric Sciences and Climate (CNR-ISAC), Bologna, Italy
[4]Department of Chemical Engineering, University of Patras, Patra, Greece

Correspondence: Satoshi Takahama (satoshi.takahama@epfl.ch), Athanasios Nenes (athanasios.nenes@epfl.ch)

S1   Size distribution of bbOA

Figure S1a shows the decrease in the OA concentration in a reference experiment (experiment 1). A first-order wall loss can explain the trend of the OA concentration well ($R^2 = 0.8$). The size distribution of OA averaged from -2 to 2 h is shown in Figure S1b. The distribution has its mode close to 200 nm for this experiment and for the majority of other experiments of this study.
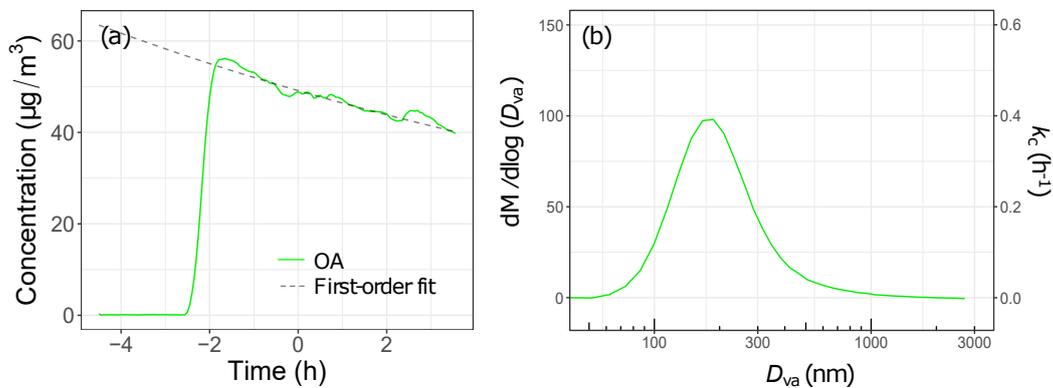
Figure S1. (a) The AMS OA concentration and the first-order fit for Exp. 1 (reference). Injection of biomass burning emissions happens at -2 h. (b) The AMS size-resolved organic mass. The results are based on particle time-of-flight (PToF) data averaged from -2 to 2 h.

S2 Investigating the volatility of lignin-like compounds

In order to ~~estimate~~ qualitatively rank the volatility of different species responsible for marker fragments, we ~~assumed that the equilibrium state in gas-particle partitioning is reached~~ interpreted thermodenuder measurements with a simplified model for a separate reference experiment (Florou et al., *in review*, 2023). This reference experiment is different from those ~~those~~ discussed in the main text. The thermodenuder design and operation is described by Gkatzelis et al. (2016) and Florou et al. (*in review*, 2023). The heating section is 50 cm in length with outer and inner diameters of 10 and 3.64 cm, respectively (the annulus is filled with sand to distribute the heat). The flow rate is 1 Lpm and the temperature profile is described by Wehner et al. (2002) and Lee et al. (2010) for similar systems. The centerline residence time was 16s at 298K (overall 32 s) in the heating section, with a residence time of 30s in the cooling section (cooled by convection).

Detailed (dynamic) modeling of the thermodenuder is described by Florou et al. (*in review*, 2023), but in this work we use a simplified approximation neglecting thermophoresis and assuming thermodynamic equilibrium at all temperatures~~and used~~, following the equation below:

$$A_i(T) = \frac{G_i(T) + A_i(T)}{1 + C_i^\star(T)/M(T)}, \tag{S1}$$

where $A_i(T)$ and $G_i(T)$ are aerosol-phase and gas-phase concentrations of the fragment i at temperature, T and $M(T)$ denotes the total organic mass. The sum of $A_i(T)$ and $G_i(T)$ are assumed to be the same between the bypass line and the thermodenuder line. The Clausius-Clapeyron equation was used to relate the saturations concentration, $C_i^\star$, at different temperatures:

$$C_i^\star(T) = \frac{298}{T} C_i^\star(298) \exp\left(\frac{\Delta H_v}{R}\left(\frac{1}{T} - \frac{1}{298}\right)\right). \tag{S2}$$

~~We neglected particle losses due to thermophoresis.~~ The total organic concentration has been assumed to be the value estimated by AMS considering a CE of unity. ΔH_v is assumed to be equal to ~~40~~ 77 kJ mol^{-1} (Florou et al., *in review*, 2023). The Levenberg-Marquardt nonlinear least-Squares algorithm was used to find the optimum $C^\star$ for different marker fragments. For $C_2H_4O_2^+$, $C_9H_{11}O_3^+$, $C_{10}H_{13}O_3^+$, CO_2^+, and $C_4H_9^+$, the $C^\star(298)$ was estimated to ~~be 5.42, 1.83, 1.32, 0.76, and 2.94~~ span one order of magnitude: 1.09, 0.3, 0.22, 0.51, and 0.1 μg m^{-3}, respectively. ~~The $C_2H_4O_2^+$ is produced by the most volatile species (levoglucosan, anhydrosugars) and the CO_2^+ by the least volatile ones. However the differences are within one order of magnitude for all the fragments above.~~ Due to simplifying assumptions (e.g., omission of thermophoresis or equilibrium state) these values should be considered ~~as order of magnitude estimates. The value of $C^\star$ estimated for the levoglucosan is slightly lower than that of Bertrand et al. (2018) but still reasonably when close considering the simplifying assumptions made here.~~

~~Time series of normalized concentrations of AMS fragments in a reference experiment (Exp. 3).~~ approximate. Changing the enthalpy changes the absolute values, but C^*s retain similar ratios, which is sufficient for our qualitative comparison.

According to this analysis, the $C_2H_4O_2^+$ is produced by the most volatile species (levoglucosan, anhydrosugars) and the CO_2^+ by the least volatile ones. As can be seen from Fig. S3, a lower loss rate is observed for $C_9H_{11}O_3^+$ in the absence of oxidants compared to other fragments including $C_2H_4O_2^+$. This suggests ~~the~~ a lower volatility of the corresponding species, as their concentration is mainly affected by particle-phase wall losses compared to particle- and gas-phase wall losses for levoglucosan. This phenomenon is observed in all experiments before the injection of oxidants.
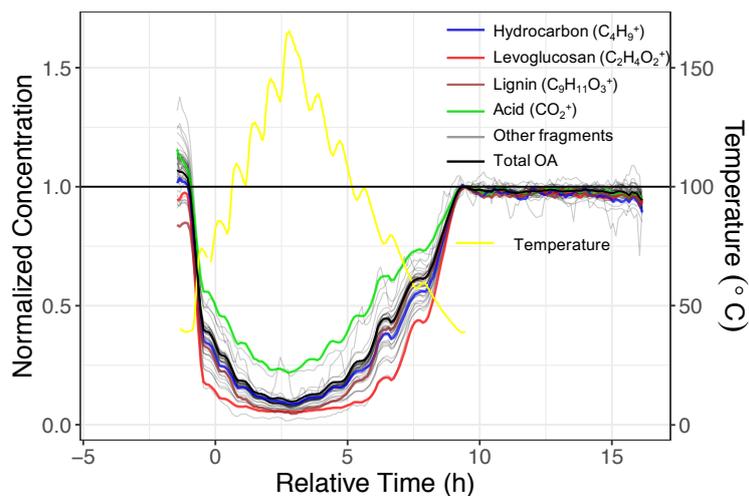
Figure S2. Concentration time series of individual AMS fragments after passing chamber OA through a thermodenuder (normalized by the concentrations through the bypass line). The temperature of the thermodenuder is shown in yellow.
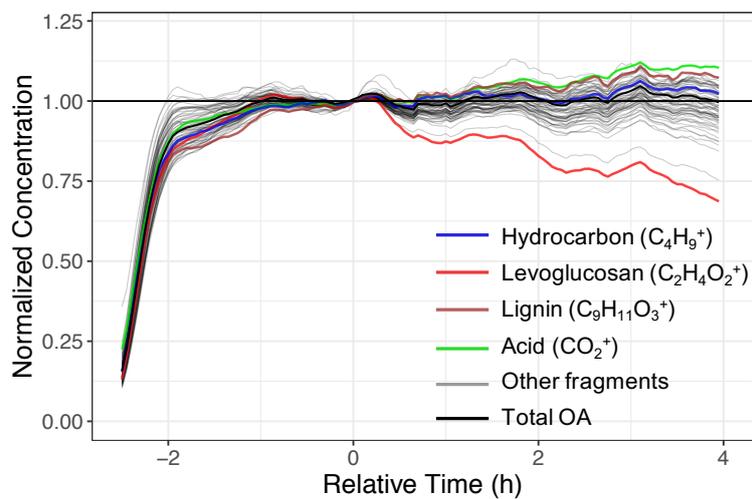
Figure S3. Time series of normalized concentrations of AMS fragments in a reference experiment (Exp. 3).

S3 AMS and FTIR comparison

40   OA concentrations estimated using FTIR and AMS are correlated ($R^2 = 0.75$; Fig. S4). Aging with UV increases the OM:OC
ratio more than aging with the nitrate radical. We also observe that the general increase in OM:OC with aging is captured by
both methods (Fig. S4c). However, the absolute values are different. PTFE filters that belong to each experiment are as follows:
Exp. 1 (filters F1, F2), Exp. 2 (F9, 10), Exp. 3 (F16, 17), Exp. 4 (F18, 19), Exp. 5 (F20, 21), Exp. 6 (F4, 5), Exp. 7 (F11, 12),
Exp. 8 (F6, 7), and Exp. (F13, 14). F3, 8, and 18 are blank filters put in the chamber for few minutes. AMS OA is not corrected

45   for the collection efficiency (CE).
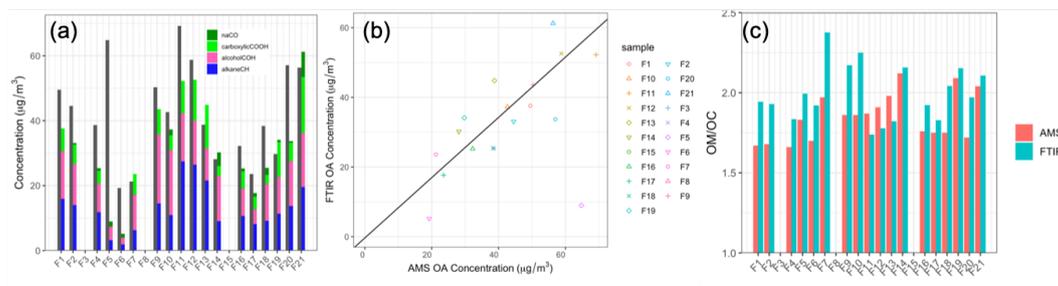
Figure S4. The OA mass concentration measured with FTIR (functional groups are color codded) and AMS (averaged over the filter sampling
periods) (a). Scatter plot comparing OA concentrations measured by AMS and FTIR (b). OM:OC ratios measured by AMS and FTIR (c).

S4 Dimension reduction of AMS mass spectra

In the figure below, the loadings of the first three principal components (up to m/z 73) for an uncentered PCA on the AMS spectra of the chamber experiments are shown. The first PC has high negative loadings of oxygenated fragments ions such as CO^+, CO_2^+, CHO^+, and $C_2H_3O^+$, showing the direction of aging. The CHO^+ fragment has a high positive loading and CO^+ and CO_2^+ have high negative loadings for PC2, suggesting that this PC distinguishes between carboxylic and dicarboxylic acids which are detected by CO_2^+ and alcohols which produce strong signals of CHO^+. This is supported by FTIR spectra of pellet burning samples which have higher PC2 scores than and strong signatures of the alcohol group than their wood burning counterparts. PC3 has high positive loadings of CO^+ and CO_2^+ and high negative loadings of $C_2H_4O_2^+$, showing the degradation of anhydrosugars with aging.
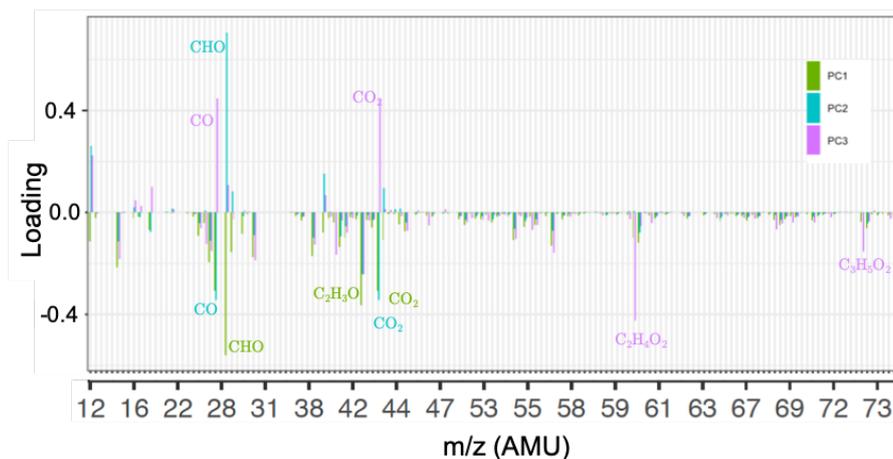
Figure S5. Loadings of the first three PCs.

 ## S5   Ammonium-subtracted spectra

In the figure below ammonium-subtracted residual spectra are shown. A reference ammonium spectrum multipled by a scaling factor, defined as the minimum ratio of each sample spectrum and reference ammonium spectrum, subtracted from the sample spectrum. CH peaks have been subtracted because there are CH peaks in the ammonium spectrum used for subtraction. Carboxylic acid and alcohol absorbances are clearly observed in these spectra.
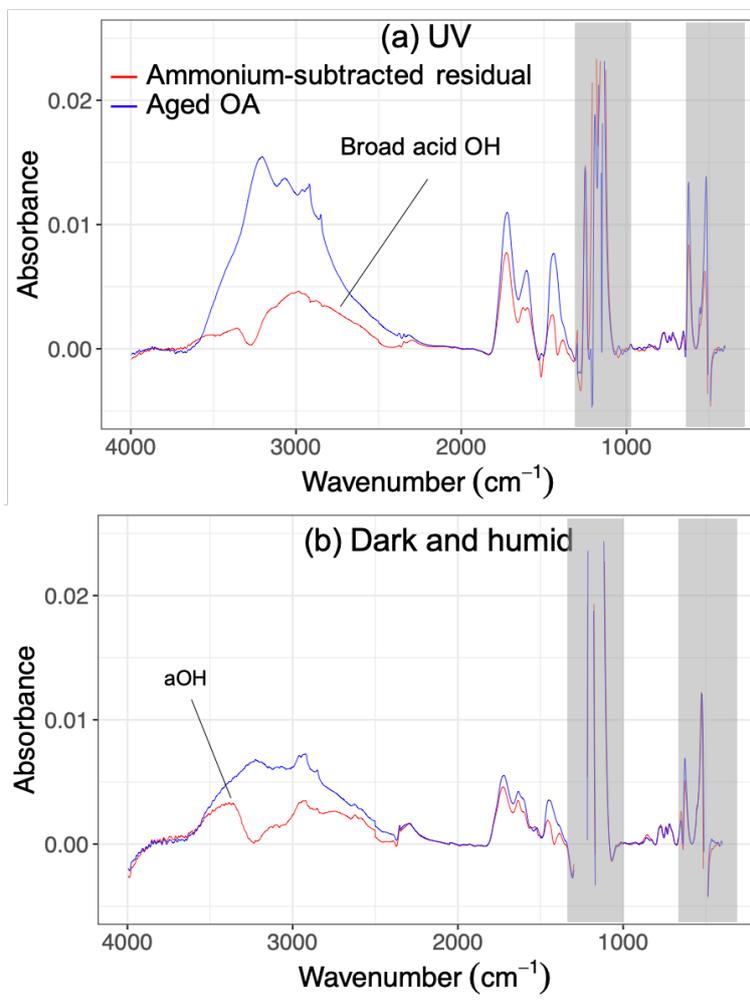
Figure S6. Ammonium-subtracted residual FTIR spectra of wood burning OA aged with UV (a) and nitrate radical (b) (Exp. 4, and 8, respectively).

S6   The FTIR spectrum of atmospheric smoke impacted PM$_{2.5}$

An example of atmospheric smoke impacted PM$_{2.5}$ samples ~~(prescribed burning in the eastern US in 2013, validated by satellite observatio~~ (prescribed burning in the eastern US in 2013, validated by satellite observations; Yazdani, 2022). High organic loading, strong acid signatures, and very weak levoglucosan and invisible lignin-like signatures are observed in the Fig. S7. Compared to primary WB aerosols in chamber, weak levoglucosan and lignin peaks in this sample are observed in the ambient spectrum. On the other hand, the broad peak from 2400–3400 cm^{-1} suggests the high abundance of carboxylic acids, which are also observed in the WB residual spectra of S6a. This observation suggest the dominant contribution of wood burning (secondary aerosols) in this atmospheric sample although primary marker are quite weak.
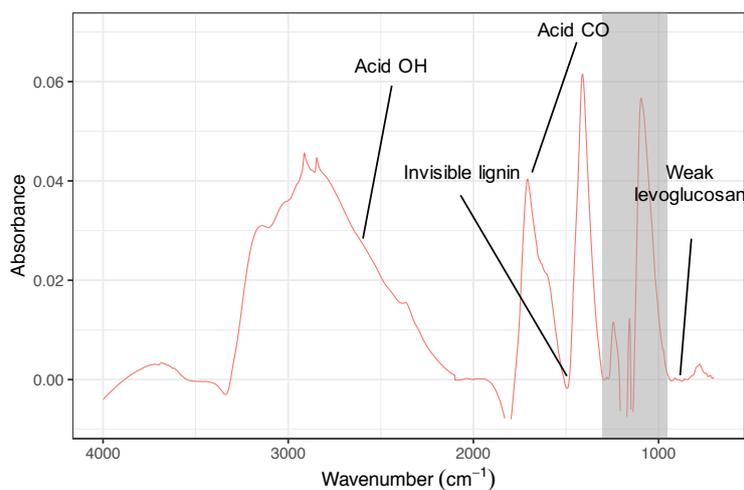
Figure S7. The FTIR spectrum of an atmospheric smoke-impacted PM$_{2.5}$ sample.

S7   Loss rates of different fragments

Based on the loss profiles for different fragments within two hours after the initiation of aging (when UV lights are on), the loss rates are estimated to be 0.38, 0.70, 0.24, and 0.23 h^{-1} for $C_2H_4O_2{}^+$, $C_9H_{11}O_3{}^+$, $C_{10}H_{13}O_3{}^+$, and $C_4H_9{}^+$.
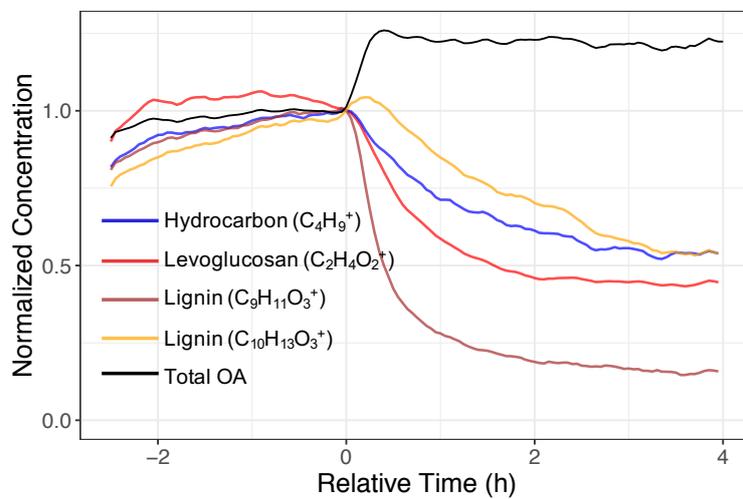
Figure S8. Smoothed time series of AMS OA concentration, and different tracer fragments in a UV experiment (Exp. 4).

70

S9

S8 $f_{44}{:}f_{43}$ ratios in residual spectra

In Fig. S9 the wall-loss corrected OA was calculated base on

$$C_{\mathrm{OA}}^{\mathrm{cor}}(t) = C_{\mathrm{OA}}^{\mathrm{obs}}(t) + k_{\mathrm{OA}} \int_{t_0}^{t} C_{\mathrm{OA}}^{\mathrm{obs}}(t)\,dt, \tag{S3}$$

where $C_{\mathrm{OA}}^{\mathrm{obs}}(t)$ is the observed (measured) OA concentration at time t, $C_{\mathrm{OA}}^{\mathrm{cor}}(t)$ is the wall-loss-corrected OA at the t, k_{OA} is the

75   first-order wall loss rate based on the AMS OA. OC was calculated from the sum of C concentration for all fragments. Dividing OA time series by OM:OC time series gives a similar trend with different absolute values.
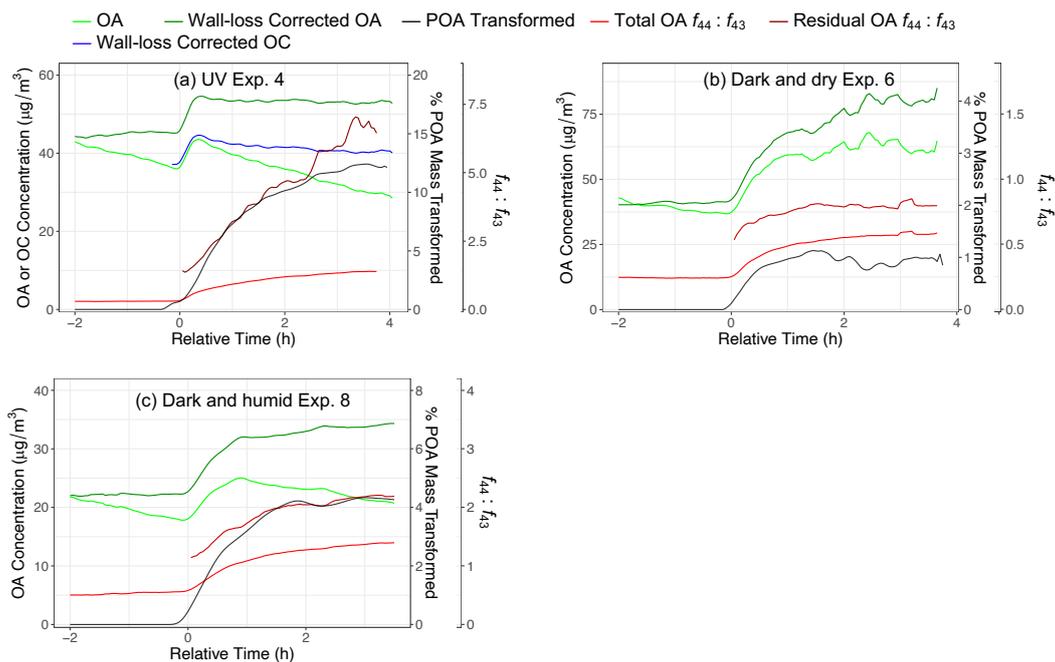
Figure S9. Time series of OA, OC concentrations, percentage of POA mass aged, and $f_{44}{:}f_{43}$ for wood burning emissions in different aging scenarios.

As can be seen from Fig. S9, the trends of POA aging and $f_{44}{:}f_{43}$ are similar in different experiments. The decrease in the OC concentration in the UV experiment with aging suggests the importance of other aging mechanisms such as photolysis in addition to the SOA condensation.

References

Bertrand, A., Stefenelli, G., Pieber, S. M., Bruns

Gkatzelis, G. I., Papanastasiou, D. K., Florou, K., Kaltsonoudis, C., Louvaris, E. A., and Pandis, S. N.: Measurement of nonvolatile particle number size distribution, Atmospheric Measurement Techniques, 9, Temime-Roussel 103–114, B. https://doi.org/10.5194/amt-9-103-2016, Slowik, J 2016.

Lee, B. G., Wortham, H., Prévôt H., Kostenidou, E., Hildebrandt, L., Riipinen, I., Engelhart, G. J., Mohr, C., DeCarlo, P. F., Mihalopoulos, N., Prevot, A. S. H., Haddad, I. E Baltensperger, U., and Marchand, Pandis, S. N.: Influence of the Vapor Wall Loss on the Degradation Rate Constants in Chamber Experiments of Levoglucosan and Other Biomass Burning Markers, Atmos. Chem. Phys., 18 Measurement of the ambient organic aerosol volatility distribution: application during the Finokalia Aerosol Measurement Experiment (FAME-2008), Atmospheric Chemistry and Physics, 10, 12 915–10149–12 930, , 2018. 160, https://doi.org/10.5194/acp-10-12149-2010, publisher: Copernicus GmbH, 2010.

Yazdani, A., Takahama

Wehner, B., Philippin, S., Raffuse, S. and Wiedensohler, A.: Design and calibration of a thermodenuder with an improved heating unit to measure the size-dependent volatile fraction of aerosol particles, Journal of Aerosol Science, 33, 1087–1093, Dillner, A. M., and Sullivan https://doi.org/10.1016/S0021-8502(02)00056-3, 2002.

Yazdani, A. P.: Identification of Smoke-Impacted PM2.5 Samples with Mid-Infrared Spectroscopy in a Monitoring Network, Manuscript in preparation, 2021. : Chemical characterization of organic aerosols with a focus on biomass burning and mid-infrared spectroscopy, Ph.D. thesis, École Polytechnique Fédérale de Lausanne, 2022.